4

Solid state spectroscopy I: IR and VUV

BL1B

Vacuum-ultra Violet Reflectance Spectroscopy of Strongly Correlated Electron System

J. Fujioka[1], S. Miyasaka[2], Y. Tokura[1,3,4]

[1]*Department of Applied Physics, University of Tokyo, Tokyo 113-8656 Japan*

[2]*Department of Physics, University of Osaka, 560-0043, Osaka Japan*

[3]*Correlated Electron Research Center (CERC), National Institute of Advance Industrial Science and Technology (AIST), Tsukuba 305-8562*

[4]*ERATO-SSS, Japan Science and Technology Agency (JST) Tsukuba 305-8562 Japan*

The spin, orbital and charge degrees of freedom in the correlated electron system have been attracting much attention. The interplay among them leads to the versatile magnetic and/or electronic structure, even though the crystal structure is nearly cubic. One interesting topic is the reconstruction of the electronic structure in the course of the insulator-metal transition, accompanying the spin/orbital ordering-disordering transition [1]. The investigation of the electronic structure over wide energy range by the measurements of the reflectivity spectra is indispensable to reveal the spin-orbital-charge coupled phenomena associated with the insulator to metal transition.

In this beamtime, we have measured the reflectivity spectra of the several transition metal oxides, including the V, Mn, Fe, Ni, and Cu ions, for an energy range between 4eV and 35eV at room temperature using the beam line BL1B. We connected the measured spectra to the low energy ones below 4 eV and calculated the optical conductivity spectra by the Kramers-Kronig analysis. As an example, we focus on the optical conductivity spectra of the single domain crystals of $Y_{1-x}Ca_xVO_3$ in this report.

The perovskite-type vanadium oxide YVO_3, which is known as the prototypical Mott-Hubbard insulator, has two valence electrons in the 3*d* orbital of the nominally trivalent V ion with the spin configuration of S=1. The orthorhombic crystal distortion splits the triply degenerate t_{2g} levels into the lower lying d_{xy} level and the higher lying doubly degenerate d_{yz} and d_{zx} ones. With lowering temperature, the Jahn-Teller distortion further lifts the degeneracy of the d_{zx} and d_{yz}, and the G-type orbital ordering (OO), where the occupied d_{zx} and d_{yz} orbitals are staggered in all (x, y, z) directions, appears at T_{OO1}=200K. Subsequently, the C-type spin ordering (SO) appears at T_{SO1}=116K, where spins align ferromagnetically along the c axis and antiferromagnetically in the ab plane. With further lowering the temperature, the C-type orbital and G-type spin ordered state appears at T_{SO2} ($=T_{OO2}$)=77K. Recent studies have revealed that the low temperature C-type orbital and G-type spin ordered phase is immediately suppressed by Ca doping, *i.e.* the hole doping as shown in fig. 1 (a).

In Fig. 1(b), we show the optical conductivity spectra of $Y_{1-x}Ca_xVO_3$ x=0 and x=0.10 for $E \parallel c$, which was measured at room temperature. In both

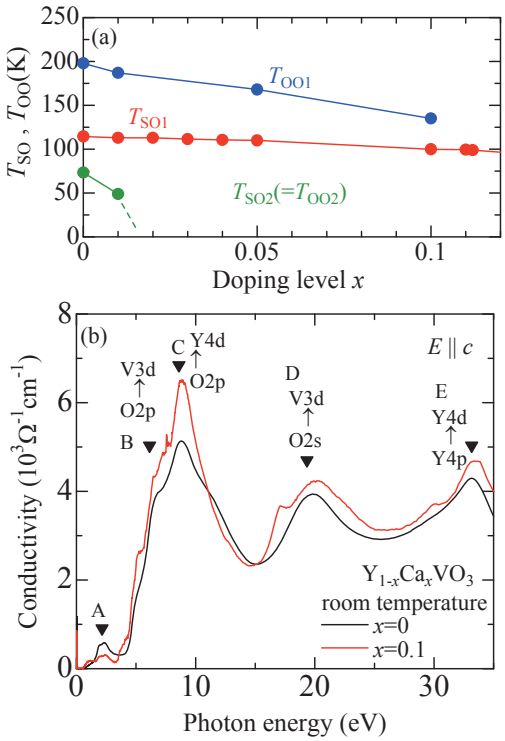

Fig. 1: (a) The spin-orbital phase diagram of $Y_{1-x}Ca_xVO_3$. (b)The optical conductivity spectra of $Y_{1-x}Ca_xVO_3$ x=0 (black line) and x=0.1 (red line), respectively.

spectra, several peaks are observed. We assigned the peak A around 2eV to the Mott-gap excitation. A more intense peak (B) is observed around 7 eV, which is assigned to the charge transfer excitation from O2*p* to V3*d* level. Above 7eV, three peaks (C, D, and E) are observed and we have assigned them to the excitations from O2*p* to Y4*d*, from O2*s* to V3*d*, and from Y4*p* to Y4*d*, respectively, according to Ref. [2]. To see the Mott gap excitation in more detail, in fig. 2, we show the magnified view of the optical conductivity spectra for YVO_3 in the low energy region. With lowering the temperature, the intensity of the Mott gap excitation for $E \parallel c$ spectra increases especially in the range of T_{SO2} ($=T_{OO2}$) < T < T_{OO1}, while that for $E \perp c$ shows minimal temperature dependence. Such an anisotropic charge dynamics is also observed in the similar system, $LaVO_3$, and is explained in terms of the quasi-one-dimensional orbital exchange interaction, which is characteristic in

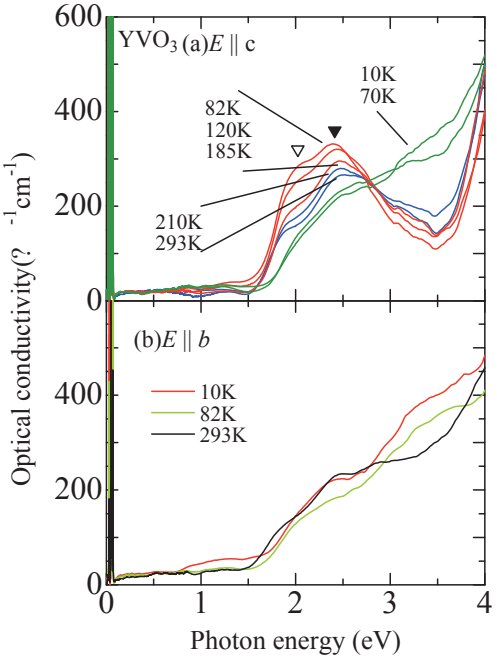

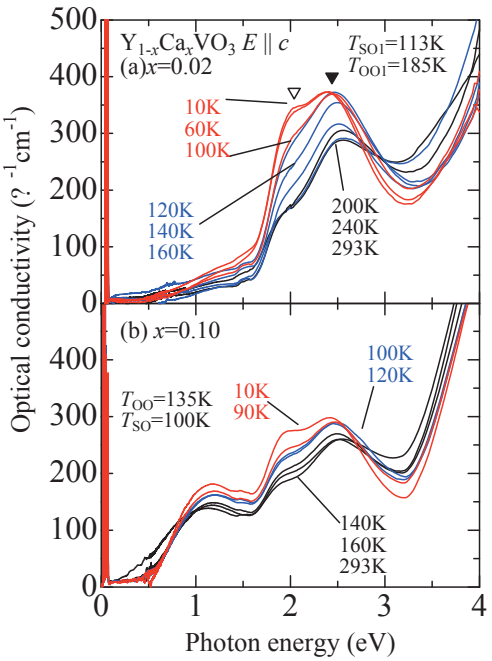

the C-type spin and G-type orbital ordered state [3,4,5]. According to the ref. [4], in the C-type spin and G-type orbital ordered phase, the Mott gap excitation is decomposed into the two components. The lower-lying band (mg1) is an allowed Mott-gap excitation along the ferromagnetic chain ($\|c$) in the C-type spin ordered state. The higher-lying band (mg2) is the nominally forbidden one, which is weakly allowed due to the imperfect spin-orbital polarization. For $T > T_{SO2}$ ($=T_{OO2}$), the intensity of mg2 seems to be larger than that of mg1, indicating the large spin and orbital fluctuation. Such kind of the large spin and orbital fluctuation in the C-type spin and G-type orbital ordered phase is also pointed out by the neutron scattering experiment [6]. On the other hand, for $T < T_{SO2}$ (T_{OO2}), the intense peak structure around 2eV disappears and the spectral weight is transferred to above 3eV. Concomitantly, the anisotropic feature of the Mott gap excitation also disappears. The disappearance of the anisotropic electronic structure may be explained in terms of the nearly isotropic orbital exchange interaction in the G-type spin and C-type orbital ordered phase.

For x=0.02, the ground state is the spin C-type / orbital G-type and the intensity of the Mott-gap excitation around 2eV in the $E\|c$ spectra increases monotonously with lowering the temperature as shown in fig. 3(a). In particular, the intensity of the mg1 continues to increase down to 10K, while there is still considerable contribution from that of mg2. This contrasts with the case of $LaVO_3$, where that of mg2 is much smaller at 10K [4]. One explanation may be that, for x=0.02, the spin and orbital quantum fluctuation is relatively enhanced compared to $LaVO_3$, since this system is located in the vicinity of the spin-orbital ordered phase boundary.

In the $E \| c$ spectra for x=0.10, the intensity of the Mott gap excitation is reduced and the additional bump structure (mid-IR peak) appears at ~1eV, which results from the incoherent motion of the doped hole as shown in fig. 3(b). The mid-IR peak for $E \| c$ spectra has larger spectral weight than that for $E \perp c$ and increases its intensity in the low temperature region, while that for $E \perp c$ shows minimal temperature dependence. Note that the spectral weight is a good measure for the kinetic energy of the electrons. For x=0.10, the orthorhombic crystal distortion is still robust and, hence, the d_{xy} level might be lower in energy than d_{yz} or d_{zx} level. Thus, as the explanation for the enhancement of the mid-IR peak for $E\|c$ spectra, it is expected that the doped holes mainly occupy the d_{yz} and d_{zx} orbitals and have a large kinetic energy along the c-axis, reflecting the quasi-one-dimensional orbital exchange interaction.

[1]M.Imada *et al.*, Rev. Mod. Phys. **70** (1998)1039.
[2] T. Arima *et al.*, J. Phys. Soc. Jpn. **64** (1995) 2488.
[3]Y. Motome *et al*, Phys. Rev. Lett. **90** (2003) 146602.
[4] S. Miyasaka *et al*, J. Phys. Soc. Jpn. **71** (2002) 2086.
[5]J. Fujioka *et al.*, Phys. Rev. Lett. **97** (2006) 196401.

BL5B

Phase Change of EUV Reflection Multilayer by Total Electron Yield and Reflection Spectra

T. Ejima, T. Harada, A. Yamazaki

Institute of Multidisciplinary Research for Advanced Materials, Tohoku University, Sendai 980-8577 Japan

In the extreme ultraviolet (EUV) wavelength region, normal incidence mirrors were made available through the use of reflection multilayers and are required to have extremely low aberrations [1]. To achieve the aberration-free multilayer mirrors, the technique of surface milling has been proposed as an accurate correction method of figure errors [2]. In order to make an accurate correction, it is important to first obtain information regarding the reflection phase in multilayer mirrors. In this study, reflection phase values for multilayer optics were obtained according to the formula derived from the total electron yield intensity and reflection in the multilayer. These phase values were found to change in accordance with increases in the thickness of the top layer.

Total electron yield (TEY) is a spectroscopic method used in X-ray regions for detecting the wavelength-dependence of the number of emitted electrons from a solid, and is proportional to the absorbed energy of the incident light in the EUV region [3]. The intensity of the photoelectrons emitted from a reflection multilayer is optically represented by three terms: incidence-, reflection-, and interference- terms [4]. When the attenuation length L of emitted photoelectrons from the top layer is smaller enough than the thickness d of the top layer, the TEY intensity $I_T(\lambda)$ is approximately represented by

$$I_T(\lambda) = I(\lambda)\left[1 + R(\lambda) + 2\sqrt{R(\lambda)}\cos\left(\delta - 2\xi(d+L)\right)\right], \quad (1)$$

where $I(\lambda)$ is a TEY spectrum of the top-layer material, R is the real part of the complex reflectance of the top layer, δ is the reflection phase at one layer below the top layer, and ξ is the real part of the top-layer's propagation-vector using angle of incidence θ, wavelength λ, and complex dielectric function ε of the top layer. The term ξ is represented as $\xi = 2\pi(\varepsilon - \sin^2\theta)/\lambda$. Equation (1) resembles the formula applied to analyze surface structures using X-ray standing waves generated by a single crystal in the hard X-ray region [5]. A phase term will be obtained on the basis of the relation to determine surface structures. As the same manner, the phase term in Eq. (1) can be represented by measurable quantities. When the phase term $\delta - 2\xi(d+L)$ is represented by Δ in Eq. (1), the cosine term difference between the thicknesses d and δd of the top layers can be obtained as

$$\cos(\Delta - 2\xi\cdot\delta d) - \cos\Delta = \left(\frac{I_T(\lambda) - I'_T(\lambda)}{I(\lambda)}\right) \Big/ 2\sqrt{R(\lambda)}. \quad (2)$$

Periodic [Mo 2.6nm/Si 4.1nm]×20 multilayers with different thicknesses of top Mo layer were fabricated on a same Si substrate. Thicknesses of the top Mo layer were accurately controlled by the shutter that was placed in front of the sample, and were deposited from 0.4nm to 3.2nm at 0.4nm intervals. A Mo single layer (d > 200nm) was also fabricated for normalization of the TEY spectra. TEY spectra of these aperiodic multilayers were measured with reflection spectra. In the measurement, a combination of the G2 grating and the M22 mirror was used for the 10-20 nm wavelength region. The incident wavelength was calibrated according to the position of the Si-$L_{2,3}$ absorption edge. The resolving power of the wavelength $\lambda/\Delta\lambda$ estimated from the width of the Si-$L_{2,3}$ absorption edge was 200. The incident light estimates include a higher order light component, with a 20% intensity component of first order light. The reflection and TEY spectra of the Mo/Si multilayer system were measured simultaneously at 10° to the normal angle of incidence.

TEY spectra of the aperiodic multilayers were normalized using the TEY spectrum of the Mo single layer. The TEY and reflection spectra are shown in Figure 1. In the TEY spectra, the main peak is observed clearly around 13.4 nm and the peak position shifts from 13.2 nm to 13.6 nm as the thickness of the top Mo layer increases. Smaller peaks are observed either side of the main peak, and the peak positions shift also to the longer wavelength region. In the reflection spectra, the series of peaks located at 13.4 nm, deviate little in their peak position despite increases in the thickness of the Mo layer.

To obtain the phase term differences, the normalized TEY spectra of each multilayer and the reflection spectra were substituted for $I_T(\lambda)/I(\lambda)$, $I'_T(\lambda)/I(\lambda)$, and $R(\lambda)$ in Eq. (2). In Figure 2, phase changes obtained experimentally are represented with those obtained numerically using the exact formula [4]. Here, the graph labels (+Mo xx nm) correspond to the top Mo layer thickness. In the calculation, the optical constants were taken from data compiled by Henke and Palik [6, 7]. The thicknesses of the periodic Mo (2.02 nm) and Si (4.76 nm) layers used

in reflection spectrum were determined by comparison of the X-ray diffraction data and fabrication conditions. The attenuation length was treated as the fitting parameter, based on NIST Standards [8]. The value of $2\xi L$ obtained from the fitting procedure was 0.3π.

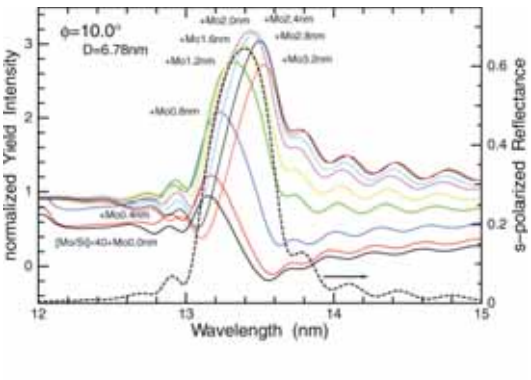

Fig. 1. Total electron yield (solid curves) and reflection (broken curve) spectra of Mo/Si multilayers with varying top Mo layer thicknesses.

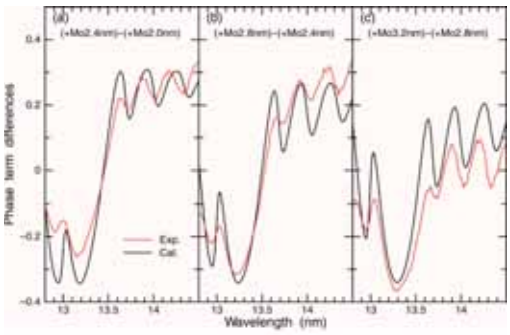

Fig. 2. Differences of the cos terms in Eq. (2). Red curves represent the experimental results and black curves, the calculation ones.

Experimental phase changes were reproduced well by the numerical simulations at that the thickness of the top Mo layer is more than 1.2nm. This result suggests that reflection phases of multilayer mirrors will be observed by both reflection and TEY spectra around reflection peaks. On the other hand, spectral shapes of the phases resemble to those of the calculation results but the values were disagreed at that the thickness of the top Mo layer is less than 1.2nm. This disagreement will be caused by overlap of photoelectrons emitted from the layers below the top layer. In other words, the assumption made on the derivation of Eq. (1), the photoelectrons are emitted from the top layer only, will not applicable in the thinner top layers.

Simultaneous reflection and TEY measurements have been obtained for aperiodic Mo/Si multilayers. The phase term differences obtained from the reflection and TEY spectra are in accordance with the change in thickness of the top Mo layer. This method will be applied to evaluate the phase information for accurate multilayer optics, for example microscopes, telescopes, and photo-masks, in the EUV region. Same phase information will be obtained from the Kramers-Kronig analysis of a reflection spectrum. The merit of this method is reliant on the TEY intensity, which can be easily measured in accordance with the corresponding reflection spectra, such that the associated phase information can be obtained for a given wavelength.

[1] For example, D. Attwood, Soft X-rays and extreme ultraviolet radiation, (Cambridge University Press, Cambridge, 2000) Chap. 4.
[2] M. Yamamoto, Nucl. Instrum. Meth. Phys. Res. A, **467-468** (2001) 1282.
[3] W. Gudat and C. Kunz, Phys. Rev. Lett., **29** (1972) 169.
[4] T. Ejima, Jpn J. Appl. Phys. **42** (2003) 6459.
[5] J. Zegenhagen, Surf. Sci. Reports, **18** (1993) 199.
[6] "Handbook of Optical Constants of Solids I, II, and III" ed. E. D. Palik, (Acad. Press. Inc., New York & London, 1985, 1991, and 1998).
[7] B. L. Henke, E. M. Gullikson, and J. C. Davis, At. Data Nucl. Data Tables 54, 181 (1993), at http://www.cxro.lbl.gov/optical_constants/.
[8] C. J. Powell and A. Jablonski, NIST Electron Effective-Attenuation-Length database, NIST standard reference database 82, (National Institute of Standards and Technology, Gaithersburg, 2001).

BL1B

Effect of Anionic Species in Ionic Liquids on Photostability

N. Inoue, M. Makita, T. Ishioka, A. Harata
Department of Molecular and Material Sciences, Kyushu University, Kasugakoen 6-1, Kasuga-shi, Fukuoka 816-8680, Japan

Photostability of ionic liquid compounds of 1-butyl-3-methylimidazolium salts was evaluated using synchrotron radiation. A remarkable change in ^{1}H-NMR and FT-IR spectra was observed for [bmim][PF_6] and [bmim][BF_4]. Production of methylimidazolium ionic liquids was confirmed. While no changes was observed for [bmim][Tf_2N]. It is suggested that photostability of ionic liquids are largely influenced by anionic species.

Introduction

Ionic liquids are defined as salts which are in the liquid state at room temperature. Ionic liquids are rapidly expanding topic of research because of their favorable properties such as negligible volatility; high chemical, thermal, and electrochemical stability; high ionic conductivity; and, in some case, hydrophobicity. These properties make them highly attractive candidates for the use in solvent for chemical reactions such as photochemistry, organic synthesis, and photocatalysis. Especially, in photochemical reaction, it is known that ionic liquids act as an electron donor or an accepter. However, photochemical behavior and any potential toxicity issues for most ionic liquids are not known, particularly with respect to alkylimidazolium systems, and preliminary data is only now being determined.

Recently, researches on water stability and thermo stability are reported. Some ionic liquids possibly decompose under moisture and high temperature atmosphere. In the case of photoreactions, presence of decomposed products might cause lowered experimental accuracy and distorted results. It is important to investigate photostability of ionic liquids precisely.

In this report, photostability and photolysis of 1-butyl- 3-methylimidazolium hexafluorophosphate, tetrafluoroborate, bis(trifluoromethanesulfonyl)imide (abbreviated [bmim][PF_6], [bmim][BF4], [bmim][Tf_2N], respectively) were investigated using synchrotron irradiation.

Experimental

The 0-th order diffraction of Seya-Namioka monochromator (10eV>) was obtained from BL1B at the UVSOR facility. The light was emitted from the chamber to a He-purged cell through an MgF_2 window. The emitted light was reflected with an Al mirror and vertically irradiated on the [bmim][PF_6] surface for 30 minutes.

These kinds of ionic liquids ([bmim][PF_6], [bmim][BF_4], [bmim][Tf_2N] (Figure 1)) were synthesized according to the literature [1-3].

Results and Discussion

In ^{1}H-NMR spectra of [bmim][PF_6], new peaks appeared at 7.5ppm (d, C-H), 7.0ppm (d, C-H), and 3.6ppm (s, N-CH_3) after SR light irradiation. These chemical shifts show that compounds like methylimidazole are formed. Similar changes were observed in [bmim][BF_4]. Figure 2 shows IR spectra of [bmim][PF_6]. New absorption peaks appeared at 1230cm^{-1}, 1285cm^{-1}, 1525cm^{-1}. These are assigned to N-CH_3 stretching vibration, N-CH_3 stretching vibration, imidazolium ring asymmetric stretching vibration, respectively. Similar changes were observed in [bmim][BF_4]. Compared to the IR spectra of methylimidazole, the products of the photolysis are assigned to methylimidazolium hexafluorophosphate ([mim][PF_6]), or methylmidazolium tetrafluoroborate ([mim][BF_4]). In contrast, [bmim][Tf_2N] did not show any change in ^{1}H-NMR and IR spectra.

It is considered that [bmim][PF_6]([bmim][BF_4]) photodecompose into [mim][PF_6]([mim][BF_4]), and 1-butene. However, no photolysis was observed in [bmim][Tf_2N]. Thus, it is apparent that photostability of ionic liquids are influenced largely by anionic species. It is considered that photolysis proceeds by nucleophilic reaction or abstraction reaction of proton. Further research including wavelength dependence will be needed.

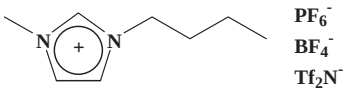

Fig. 1 Structure of [bmim][PF_6], [bmim][BF_4], and [bmim][Tf_2N].

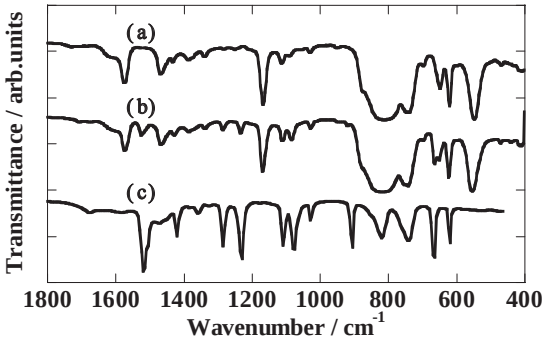

Fig. 2 IR spectra of (a) [bmim][PF_6], (b) [bmim] [PF_6] after SR light irradiation, and (c) methyl imidazole.

[1] J. G. Huddleston, R. D. Rogers, Chem. Commun (1998) 1765
[2] Rika. Hagiwara, Yasuhiko Ito, Journal of Fluorine Chemistry **105** (2000) 221
[3] M.J.Earle, C.M.Gordon, K.R.Seddon, Analytical Chemistry (2006) 6

BL1B

Photoluminescence from Localized Excitons in $PbCl_2$, $PbCl_2$:Br^- and $PbCl_2$:I^- Crystals

S. Izuhara[1], M. Kitaura[2], H. Nakagawa[1]
[1]*Dep. of Electrical & Electronics Engineering, Fukui University, Fukui, 910-8507*
[2]*Fukui National College of Technology, Sabae, 916-8507*

The excitonic states of lead halides are represented by the excited states of a Pb^{2+} ion in rough approximation. Indeed, since the optical properties are strongly dependent on halogen species, the excitonic states certainly include significant contribution from electronic orbitals of halogen. It has been accepted that the outermost p orbitals of halogen play an important role in self-trapping of excitons in PbX_2 (X=F, Cl, Br). As is well known, the information on absorption and luminescence of the halide crystal doped with other halogen ion impurity is indispensable to see the relaxed configuration of self-trapped excitons (STE's) in the host crystal. The purpose of the present study is to investigate the localized exciton luminescence of $PbCl_2$ crystals doped with a small amount of Br^- ions and I^- ions.

Special reagent grade powder of 99.99% purity of dehydrated $PbCl_2$, $PbBr_2$ and PbI_2 were purchased from Kojundo Chemical Laboraty. The single crystals of $PbCl_2$, $PbCl_2$:Br^- (0.01mol%) and $PbCl_2$:I^-(0.01mol%) were grown from melt in sealed quartz ampoules by the Bridgeman method. Samples were cut in the size of 5×5×5 mm^3 from crystal ingots with a razor blade. The mesurements of emission and excitation spectra were carried out at BL1B using a normal incidence monochromator. Photoluminescence from samples was guided into the incident slit of a grating monochromator by a optical fiber, and then detected by a CCD detector or a photomultiplier tube. The crystal samples were mounted on the copper holder of a closed-cycle He refigerator in order to perform measurements at 13K.

Figure 1 shows emission spectra of $PbCl_2$, $PbCl_2$:Br^-, and $PbCl_2$:I^- at 13K (black lines). The excitation spectra for the emission bands observed in the three samples are also indicated by red lines. In the crystal of $PbCl_2$, two emission bands are observed at 3.78eV (UV emission) and 2.89eV (B emission) under excitation at 4.6 eV. This spectrum is in agreement with the emission spectrum previously reported [1] .

In the crystal of $PbCl_2$:Br^-, three emission bands are observed at 3.1eV (V_1 emission), 2.32eV (G emission) and 1.75eV (R emission) by photostimulation at 4.3eV. The V_1 emission is strongly excited in the narrow energy region around 4.3eV (shaded area), which is located in the low energy tail of the fundamental abosrption in $PbCl_2$.

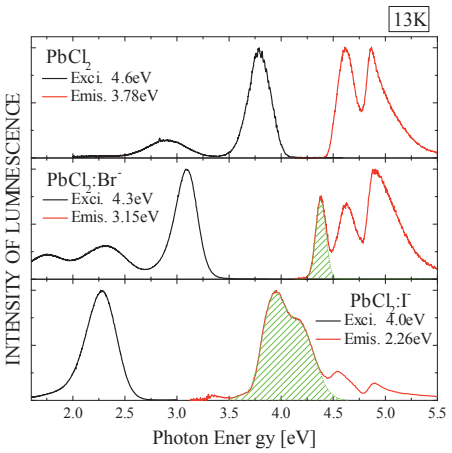

Fig.1 Emission spectra (black lines) and excitation spectra (red lines) of $PbCl_2$, $PbCl_2$:Br^-, and $PbCl_2$:I^- .

In the crystal of $PbCl_2$:I^-, an emission band appears at 2.26eV (Y emission) when the excitation photon energy is adjusted at 4.0 eV. The Y emission is also excited in the limited energy region around 4.0eV (shaded area), which separates from the intrinsic absorption edge.

It seems that the V_1 emission in $PbCl_2$:Br^- and Y emission in $PbCl_2$:I^- are similar to the luminescence from localized excitons in Br^- or I^- doped alkali chlorides, in the sense that the excitation for the emission takes place in the energy region below the excitonic absorption band of the host lattice. They are assigned to the luminescence from localized excitons.

According to the cluster calculation, the excitonic states of lead halide are described by a complex molecule of lead and halogen ions. We expect that the wave function of an electron is localized on a lead ion while that of a hole is distributed on the adjacent halogen ions in $PbCl_2$:Br^- and $PbCl_2$:I^-. The cluster calculation by the DV-Xα method is now under proceeding to make sure of our expectation.

[1] M.Kitaura *et al*., J. Phys. Soc. Jpn. **70** (2001) 2462.

BL1B

Luminescence and Excitation Properties of Host Lattice and Eu^{2+} Ions in $BaMgAl_{10}O_{17}$:Eu Phosphor

H. Yoshida[1,2], H. Kai[1], S. Watanabe[1], K. Ogasawara[1]

[1]*Department of Chemistry, Kwansei Gakuin University, 2-1 Gakuen, Sanda, 669-1337, Japan*

[2]*Research and Development Division, NEC Lighting, Ltd., 3-1 Nichiden, Minakuchi-cho, Koka, 528-8501, Japan*

From the view points of the importance as an efficient blue-emitting phosphor, $Ba_{1-x}Eu_xMgAl_{10}O_{17}$ (BAM:Eu) is a material of great interest in the recent research of phosphor. It is well known that BAM:Eu phosphor used for 3-band fluorescent lamps (FLs) and color plasma displays (PDPs) exhibit a decrease of luminescence and color shift due to thermal and discharge damage. Therefore, their products have been many issues in using it.

The blue emission in BAM:Eu is due to the $4f^65d^1 \rightarrow 4f^7$ transition of Eu^{2+} ions. As substituted location of Eu^{2+} ions, three sites are generally considered in the host lattice. The Beevers-Ross(BR) site is originally located to the Ba^{2+} site, while the anti-Beevers-Ross (aBR) and the mid-oxygen (mO) sites are in the interstitial positions[1]. According to recent reports, the most dominant site of Eu^{2+} ions in BAM is considered to be aBR[2-5]. However, this problem is still in controversy.

In this report, we have investigated the excitation properties of host lattice and Eu^{2+} ions in BAM:Eu phosphor by using the technique of vacuum ultraviolet measurements by synchrotron radiation light and first-principles molecular orbital calculation method developed for rare earth ions.

The luminescence bands at about 258 nm and 450 nm, which originate from the host lattice and the Eu^{2+} ions in BAM:Eu respectively, are observed. Figure 1 shows normalized excitation spectra of BAM:Eu. For x = 0, two excitation peaks at 160 nm and 175 nm are observed. They are considered to be due to the O 2p → Ba 5d transitions and the O 2p → Al 3d transitions within spinel block, respectively [6]. The excitation spectra at 450-nm emission band show a significant absorption band at 200 nm as well as the two main structures peaking at 310 nm and 250 nm. It is well known that the excitation band between 220 nm and 380 nm clearly increases with an increase of the amount of Eu^{2+} ions, which is due to $4f^7 \rightarrow 4f^65d^1$ transitions of Eu^{2+} ions. It is also found that the absorption edge of host lattice at 190 nm is unchanged with increase of Eu content, which indicates that the absorption of Eu activator center in BAM does not overlap that of the host lattice. On the other hand, in the luminescence spectrum under the excitation at 200 nm, the 388-nm emission band with an extrinsic characteristic was strongly observed, while the electronic state calculation of Eu^{2+} site in BAM:Eu suggested a possible contribution of the mid-oxygen sites in BAM:Eu [4,5] to this 200-nm structure. Therefore, in addition to the mO site, the present results indicate that some kind of defects or impurities also contribute to the 200-nm structure.

[1] N. Iyi, Z. Inoue and S. Kimura, J. Solid State Chem. **61** (1986) 236.

[2] K. C. Mishra, M. Raukas, A. Ellens and K. H. Jhonson, J. Lumin. **96** (2002) 95.

[3] M. Stephan, P.C.schmidt, K.C. Mishra, MRaukas, A. Ellens and P. Boolchand, Z. Phys. Chem. **215** (2001) 1397.

[4] H. Toyoshima, S. Watanabe, k. Ogasawara and H. Yoshida, J. Lumin. **122-123** (2007) 104.

[5] H. Yoshida, T. Yamazaki, H. Toyoshima, S. Watanabe, K. Ogasawara and H. Yamamoto, J. Electrochem. Soc., submitted.

[6] B. Howe and A.L. Diaz, J. Lumin. **109** (2004) 51.

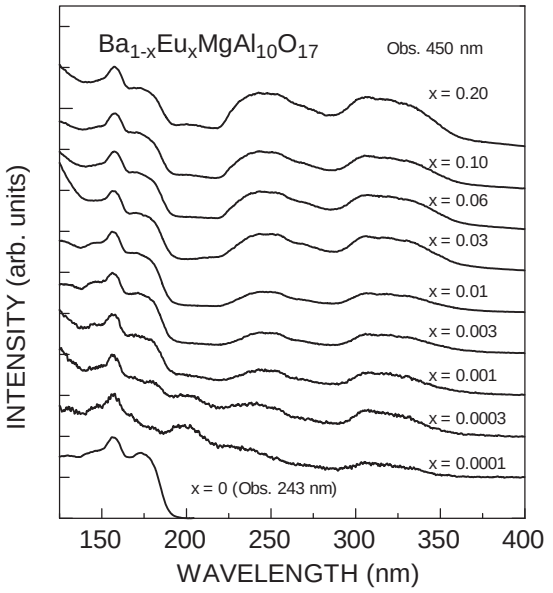

Fig. 1 Excitation spectra of $Ba_{1-x}Eu_xMgAl_{10}O_{17}$ (x = 0.0001, 0.0003, 0.001, 0.003, 0.01, 0.03, 0.06, 0.1, 0.2) observed at 450-nm emission band. As reference, an excitation spectrum of the 243-nm emission in x = 0 is also shown.

BL1B

Excitation Energy Transfer in CeF_3 Crystals Heavily Doped with Sr^{2+} Ions

Y. Tani, T. Katagiri, D. Iri, M. Itoh, M. Fujita[1], A. Yoshikawa[2], K. Aoki[3]
Department of Electrical and Electronic Engineering, Shinshu University, Nagano 380-8553
[1]Japan Coast Guard Academy, Kure 737-8512
[2]Institute of Multidiscriplinary Research for Advanced Materials, Tohoku University, Sendai 980-8577
[3]Stella Chemifa Corporation, 1-41 Rinkai-cho, Izumiootsu, Osaka 595-0075

Among single-component fluorides such as BaF_2, CaF_2, CeF_3, etc., CeF_3 is one of the most commonly used crystalline scintillating materials with fast decaying luminescence. In the present paper, excitation energy transfer in CeF_3 crystals doped with Sr^{2+} ions is discussed.

Experiment

CeF_3 single crystals heavily doped with Sr^{2+} ions (3 mol%) were grown by the micro-pulling-down (μ-PD) method [1]. Three dimensional emission (λ_{em})-excitation (λ_{ex}) spectra were measured using a SpectraPro-300i monochromator equipped with an LN/CCD camera. The decay kinetics of luminescence was detected by an MCP with use of a time-correlated single-photon counting technique when the UVSOR storage ring was operating in single-bunch mode (pulse width: 1.3 ns; pulse interval: 177.6 ns).

Results and Discussion

Figure 1 shows the contour plots of emission-excitation spectra of CeF_3:Sr at (a) 8 K and (b) 300 K. In Fig. 1(a) an emission band peaking around 330 nm is excited with UV light at $\lambda_{ex} < 290$ nm. This band somewhat red-shifts relative to the Ce^{3+} 5d → 4f luminescence (287 and 304 nm) in pure CeF_3. The excitation threshold (290 nm) is also lowered as compared to that (260 nm) for the intrinsic Ce^{3+} luminescence. These facts suggest that the 330 nm band is ascribed to Ce^{3+} ions perturbed by nearby Sr^{2+} ions. The intrinsic Ce^{3+} luminescence locating on the short-wavelength side of the main band at 330 nm is very weak in intensity due to heavy doping.

In Fig. 1(b) an emission band appears at around 400 nm at the expense of the 330 nm band. The 400 nm band, which is excited at $\lambda_{ex} < 295$ nm, is probably attributed to some defect that was introduced by Sr^{2+} doping. Therefore, it is supposed that excitation energy is efficiently transferred from Ce^{3+} sites to defect sites when the CeF_3:Sr crystal is warmed from 8 to 300 K.

Figure 2 shows the decay behaviors of (a) the 330 nm luminescence at 8 K and (b) the 400 nm luminescence at 300 K, both being excited at $\lambda_{ex} = 266$ nm. The two bands exhibit a single exponetial decay over two decades. The decay times of the 330 and 400 nm bands are 26 and 40 ns, respectively. These values are comparable with the decay time (17 ns at 8 K) of the intrinsic Ce^{3+} luminescence.

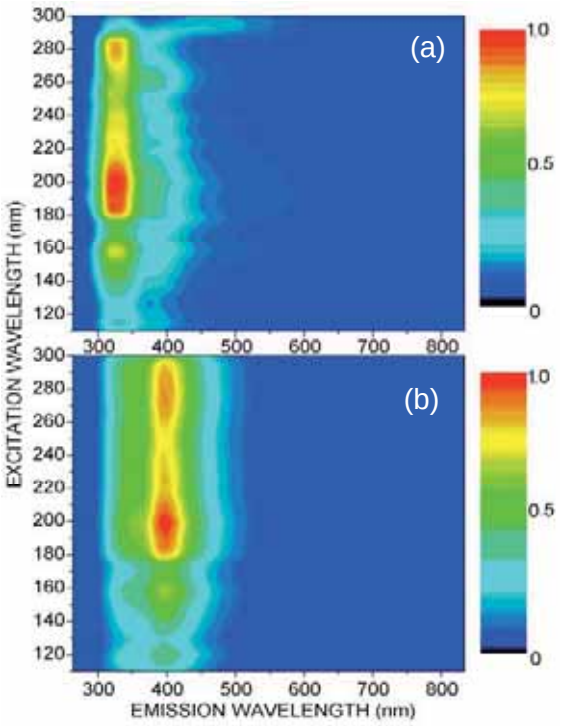

Fig. 1. Contour plots of the emission-excitation spectra of CeF_3:Sr at (a) 8 K and (b) 300 K.

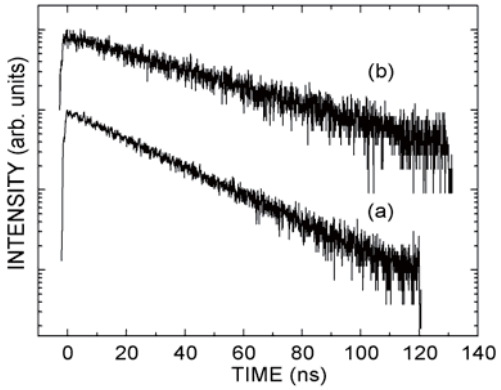

Fig. 2. Decay curves of (a) the 330 nm luminescence at 8 K and (b) the 400 nm luminescence at 300 K.

[1] A. Yoshikawa, et al.: J. Cryst. Growth **270** (2004) 427.

BL1B

Energy Transfer to Pr^{3+} Ions in LuAG:Pr Crystals

T. Katagiri, D. Iri, M. Itoh, M. Fujita[1], A. Yoshikawa[2], H. Ogino[2], K. Kamada[2]

Department of Electrical and Electronic Engineering, Shinshu University, Nagano 380-8553
[1]Japan Coast Guard Academy, Kure 737-8512
[2]Institute of Multidiscriplinary Research for Advanced Materials, Tohoku University, Sendai 980-8577

In the last decade, $Lu_3Al_5O_{12}$ (LuAG) garnet doped with rare-earth ions attracts much attention as an effective scintillating material. Pr^{3+}-doped $Lu_3Al_5O_{12}$ is a newly-grown crystal in the LuAG family. Therefore, a search for its luminescence properties is very interesting. In this work, we have investigated three dimensional (3-D) emission-excitation spectra and luminescence decay kinetics of LuAG:Pr crystals.

Experiment

Single crystals of LuAG:Pr (0.3 mol%) were grown by the micro-pulling-down (μ-PD) method [1]. The 3-D emission (λ_{em})-excitation (λ_{ex}) spectra were measured by using an Acton SpectraPro-300i monochromator equipped with a camera (Roper Scientific LN/CCD-100EB-GI). Luminescence decay kinetics was detected by an MCP (Hamamatsu R3809U-52) with use of a time-correlated single-photon counting technique under the single-bunch operation of the UVSOR ring (duration: 1.3 ns; interval: 177.6 ns).

Results and Discussion

Figure 1 shows the 3-D spectrum of LuAG:Pr at 8 K. Three broad emission bands are observed at 260, 310 and 370 nm. The 260 nm band is the intrinsic luminescence of LuAG, because it is excited with UV light above the fundamental absorption edge (λ_{ex} < 172 nm). The 310 and 370 nm bands are ascribed to the 5d → 4f transitions of Pr^{3+} ions. In the region at λ_{em} > 400 nm, several weak emission lines are seen and attributed to the 4f → 4f transitions of Pr^{3+} ions.

The decay behaviors of the 310 nm luminescence excited at 280 and 170 nm are shown in Figs. 2(a) and 2(b), respectively. Under the direct 4f → 5d excitaion of Pr^{3+} ions (a), the emission intensity decays single-exponentially over two orders of magnitude, with a lifetime of 18.4 ns. When the host crystal is photoexcited (b), two remarkable changes take place in the decay kinetics. One is that a rise componet appears in the initial stage at t = 0, as seen from the insets of Fig. 2. The other is that a piled-up component apparently increases in intensity.

The above facts strongly suggest that there are two kinds of energy transfer mechanisms from the host LuAG crystal to the Pr^{3+} ions; a fast process with a transfer time τ_T of nanoseconds or less and a slow process with τ_T > 1 μs. These transfer processes are not so sensitive to the temperature, because the decay behaviors at 300 K are almost the same as Fig. 2.

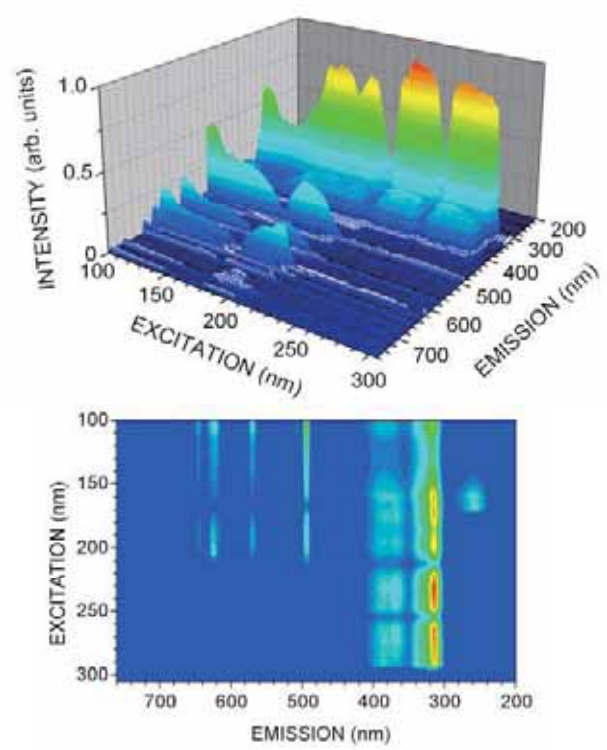

Fig. 1. 3-D emission-excitation spectrum of LuAG:Pr at 8 K, together with the contour plot of the upper spectrum in the (λ_{em}, λ_{ex}) plane.

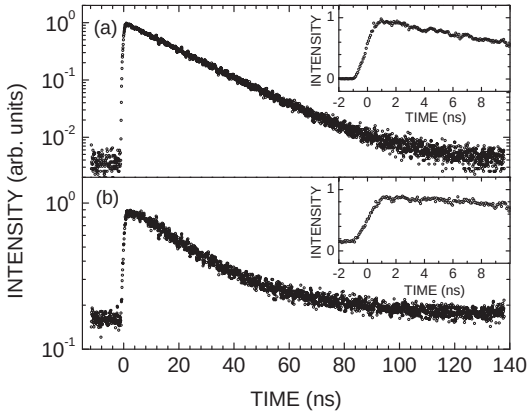

Fig. 2. Decay behaviors of the 310 nm luminescence of LuAG:Pr excited at (a) 280 and (b) 170 nm at 8 K.

[1] H. Ogino, A. Yoshikawa, et al., J. Cryst. Growth **287** (2006) 335.

Luminescence Properties of Heavily Doped CsI:Tl$^+$ Crystals

T. Kawai[1], T. Hirai[2], N. Ohno[2,3]

[1]*Graduate School of Science, Osaka Prefecture University, Sakai 590-0035, Japan*
[2]*Academic Frontier Promotion Center, Osaka Electro-Communication University*
[3]*Graduate School of Engineering, Osaka Electro-Communication University, Neyagawa 572-8530, Japan*

CsI crystals doped with Tl^+ ions exhibit complicated luminescence properties in the different way from the Tl^+ centers doped in NaCl-type alkali halides. The two UV bands are attributed to intra transition of the Tl^+ ion. The two visible-light bands are considered to originate from the Tl^+ perturbed self-trapped excitons [1]. In order to determine the characteristics of the complicated luminescence and their origin, the luminescence properties of CsI:Tl^+ crystals with various Tl^+ concentrations have been studied [2]. In the present study, we have investigated luminescence properties of the heavily doped CsI:Tl^+ crystals in order to clarify an influence of the Tl^+ concentration on the luminescence characteristics.

Single crystals of the heavily doped CsI:Tl^+ were grown from a starting material with the concentration of 1.0 mol% TlI by Bridgmann method. Luminescence and excitation spectra of the CsI:Tl^+ crystals were measured at the BL-1B beam line of UVSOR.

Figure 1 shows the luminescence spectra of the heavily doped CsI:Tl^+ crystal at 10K under the excitation on 4.30 and 4.00 eV. Under the excitation on 4.30 eV, which corresponds to the peak energy of the A absorption band of CsI:Tl^+, the luminescence bands are observed around 2.21, 2.52, and 3.05 eV. The bands are the same ones of the CsI:Tl^+ crystals with the concentration of less than 10^{-3}mol%. When the concentration of the Tl^+ ions is 1.0 mol%, the absorption intensity around the energy region below 4.30 eV increases remarkably. In the heavily doped CsI:Tl^+ crystal, the 4.00 eV excitation causes the new luminescence bands peaking at 2.05, 2.31 and 2.73 eV.

Figure 2 shows the excitation spectra 2.03 and 2.25 eV of the heavily doped CsI:Tl^+ crystal. The excitation spectrum for 2.25 eV is similar to that of the CsI:Tl^+ crystals with the concentration of less than 10^{-3}mol%. On the other hand, the excitation spectrum for 2.03 eV exhibits the strong response at 4.10 eV, which corresponds to the energy region below the A absorption band.

In general, as the concentration of the Tl^+ ions increases beyond 10^{-2} mol%, aggregate centers such as dimer are created [3]. The absorption bands due to the aggregate centers are observed in the energy region below the A absorption band. Since the 2.05 eV luminescence band in the heavily doped CsI:Tl^+ crystal has the strong response in the lower energy region than the A band, the 2.05 eV band should be attributed to the aggregate centers of the Tl^+ ions. The aggregate centers would exhibit the different characteristics of the luminescence from the isolated Tl^+ centers.

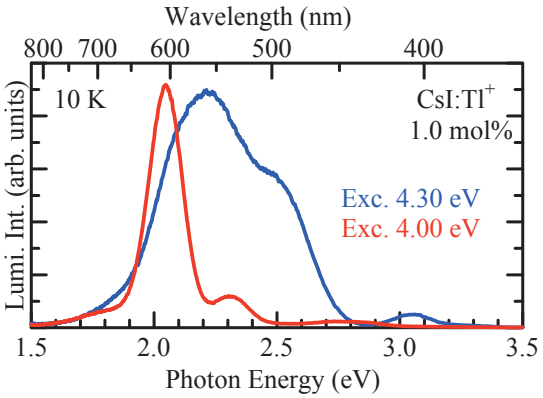

Fig. 1. Luminescence spectra of the heavily doped CsI:Tl^+ crystal under the excitation on 4.00 eV (red curve) and 4.30 eV (blue curve).

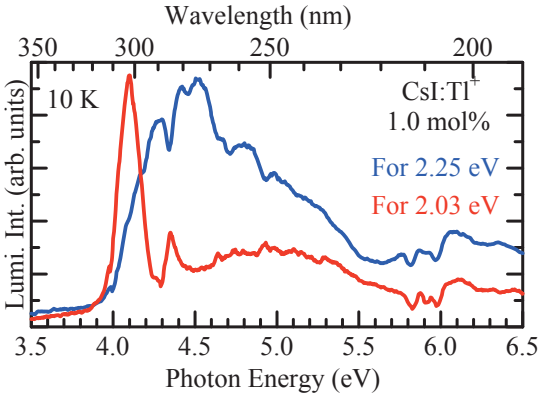

Fig. 2. Excitation spectra for 2.03 eV (red curve) and 2.25 eV (blue curve) of the heavily doped CsI:Tl^+ crystal.

[1] V. Nagirnyi, S. Zazubovich, V. Zepelin, M. Nikl and G. P. Pazzi, Chem. Phys. Lett. **227** (1994) 533.
[2] V. Babin, A. Krasnikov, H. Wieczorek and S. Zazubovich, Nucl. Instr. and Meth. in Phys. Res. A **486** (2002) 486.
[3] T.Tsuboi and P.W.M.Jacobs, J. Phys. Chem. Solids **52** (1991) 69.

BL1B

Luminescence Properties of $YPO_4:Bi^{3+}$

N. Ohno, T. Hirai

Academic Frontier Promotion Center,
Osaka Electro-Communication University, Neyagawa, Osaka 572-8530, Japan

Metal ions with s^2 electronic configurations doped in wide-gap materials such as alkali halides, which are called Tl^+-type ions, show several strong absorption bands due to $s^2 \rightarrow sp$ transitions. Since these optical transitions are dipole-allowed, the absorption is expected to be much stronger than that due to the dipole-forbidden *f-f* transitions in rare-earth ions.

Xe dimer (Xe_2) discharge fluorescent lamp is one of the candidates for alternative lighting sources to a conventional Hg discharge fluorescent lamp. New phosphors suitable for the conversion of vacuum ultraviolet (VUV) light into visible light are quite desired at present. In the Xe_2 discharge florescent lamps, phosphors are excited by VUV light of 7.2 and 8.4 eV. Most fluoride and phosphate hosts are transparent up to ~ 10 eV, so that the VUV light can directly excite impurity activators in these hosts. The strong absorption would give efficient conversion of the VUV light from the Xe_2 discharge fluorescent lamps.

In the present study, luminescence properties of trivalent Tl^+-type Bi^{3+} centers in phosphate and fluoride hosts have been studied in the UV and VUV region. The $YPO_4:Bi^{3+}$ and $YF_3:Bi^{3+}$ phosphors were prepared by amounts of the appropriate starting compound powders of YPO_4 and YF_3 adding BiF_3 (~ 2 mol %), mixing and firing in a carbon crucible at 900ºC in argon atmosphere. Impurity Bi^{3+} ions would be expected to be substituted for Y^{3+} ions in the host lattices.

Figure 1 shows luminescence (blue curve) and photo-excitation (red curve) spectra of $YPO_4:Bi^{3+}$ measured at room temperature. Luminescence peaks located at 3.1 eV and 3.6 eV and a small hump at 4.9 eV are observed for the excitation of VUV light at 7.8 eV. The 3.1 and 3.6 eV luminescence is excited with photons of 5.4 eV and the luminescence energies of Xe discharge lamp in the VUV region. These excitation peaks are located at lower energies than the absorption edge of the host YPO_4 (~ 12 eV). Therefore, the observed luminescence bands of $YPO_4:Bi^{3+}$ would be responsible for intra-ionic transitions in impurity Bi^{3+} ions.

Tl^+-type ions doped in alkali-halide crystals with a high symmetry crystal structure exhibit three characteristic absorption bands arising from the $s^2 \rightarrow sp$ transitions, namely, A, B and C bands [1]. These absorption bands have been attributed to the optical transition from the $^1S_0$ ground state to $^3P_1$, $^3P_2$, and $^1P_1$ excited states, respectively. Kang *et al*. have reported that the A and C bands appear at 3.7 and ~ 6.0 eV, respectively, in the absorption spectrum of $KCl:Bi^{3+}$ at low temperatures [2].

In Bi^{3+} ions doped in phosphate and fluoride hosts, the absorption bands would shift to the higher energy side, as compared to those in chloride hosts. In $YPO_4:Bi^{3+}$ crystals, the excitation band appearing at 5.4 eV is tentatively assigned as the A band nature due to $^1S_0 \rightarrow {}^3P_1$ transition in Bi^{3+} ions. The excitation bands at 6.5–10 eV show composite structures, which is a common feature of the C band of Tl^+-type ions. Therefore, these structures in the VUV region is ascribed to the C band origin ascribed to $^1S_0 \rightarrow {}^1P_1$ transitions in Bi^{3+} ions.

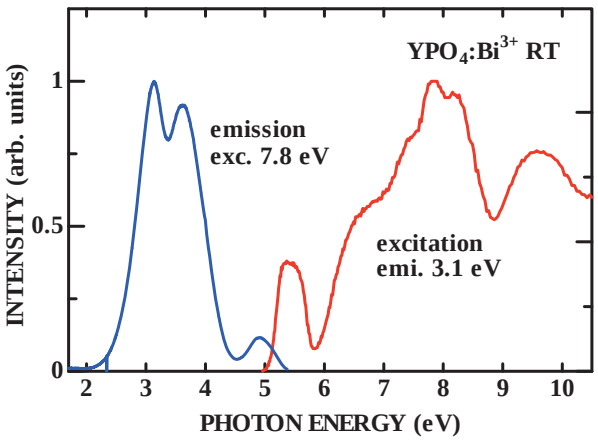

Fig. 1. Luminescence (blue curve) and excitation (red curve) spectra of $YPO_4:Bi^{3+}$ at room temperature.

[1] W.B. Fowler, *Physics of Color Centers,* Academic Press Inc., New York, 1968.
[2] J.G. Kang, H.M. Yoon, G.M. Chun, Y.D. Kim and T. Tsuboi, J. Phys.: Condens. Matter **6** (1994) 2101.

BL1B

Photoluminescence of Hydroxyapatite Irradiated by Ultraviolet Synchrotron Orbital Radiation Light (3)

M. Ohta

Department of Material Science and Technology, Faculty of Engineering, Niigata University, 8050 Ikarashi 2-no-cho, Niigata 950-2181, Japan

It was known that rare earth ions dosed for oral administration to mouse and rat are transferred to blood vessel through the ileum and deposited its teeth and bone, which mainly consists of hydroxyapatite ($Ca_{10}(PO_4)_6(OH)_2$) [1-2]. Recently, rare earth is also useful as a contrast medium for magnetic resonance imaging, restriction enzyme, biocatalyst, and so on in fields of biochemistry, physiology, medicine, etc. However, the behavior of rare earth in the living body system remains an open question until now. We have found that Eu ion substituted Ba ion in Eu doped $Ba_{10}(PO_4)_6Cl_2$ phosphor, which matrix is apatite structure[3]. The rare earth ion is also found to substitute easily for calcium ion in hydroxyapatite which is soaked in rare earth chloride aqueous solution, and to play on emission center.

In this study, hydroxyapatite samples doped with rare earth phosphate were prepared in order to apply to phosphor. Their characteristics were investigated by photoluminescent property of rare earth ion-doped hydoxyapatite samples excited by ultraviolet synchrotron orbital radiation light.

Eu-doped hydroxyapatite and Gd-doped hydroxyapatite samples were prepared as follows: hydroxyapatite was added with $EuPO_4$ or $GdPO_4$ and mixed homogeneously, and then heated at 1373K for 1 hr. $EuPO_4$ or $GdPO_4$ was prepared by reaction of $GdCl_3$ or $YbCl_3$ and $Na_3PO_4 \cdot 12H_2O$ and then fired at 1373K for 1 hr. $GdCl_3$ or $YbCl_3$ was prepared by reaction of Eu_2O_3 or Gd_2O_3 and HCl.

The photoluminescent property of each sample exited by ultraviolet synchrotron orbital radiation light (BL-1B) was detected by using with a multi-channel analyzer.

Figure 1 shows photoluminescence spectra of rare earth ion-doped hydroxyapatite samples excited by BL-1B.

The data of X-ray powder diffraction indicated that the rare earth ion substituted for calcium ion in hydroxyapatite.

Figure 1 shows the photoluminescent spectra of rare earth ion-doped hydroxyapatite samples excited by ultraviolet synchrotron orbital radiation light. In Eu ion-doped sample, 4 peaks due to $^5D_0 \rightarrow {}^7F_1$ (595nm), $^5D_0 \rightarrow {}^7F_2$ (612nm), $^5D_0 \rightarrow {}^7F_3$ (654nm), and $^5D_0 \rightarrow {}^7F_4$ (700nm) of Eu^{3+}, and 3 broad peaks (at near 330nm, 430nm and 580nm) due to hydroxyapatite matrix. The emission intensity of Eu^{3+} ion was very weak.

In Gd ion-doped sample, a peak due to $^6P_{7/2} \rightarrow {}^8S$ (320nm) and 3 broad peaks (at near 330nm, 430nm and 580nm) due to hydroxyapatite matrix.

[1] S. Hirano, K. T. Suzuki, Environ. Health Perspect. **104** (Supplement 1) (1996) 85.
[2] K. Kostial, B. Kargacin, M. Lendeka, Int. J. Radiat. Biol. Relat. Stud. Phys. Chem. Med. **51** (1987) 139.
[3] M. Sato, T. Tanaka, M. Ohta, J. Electrochem. Soc.,**141** (1994) 1851.

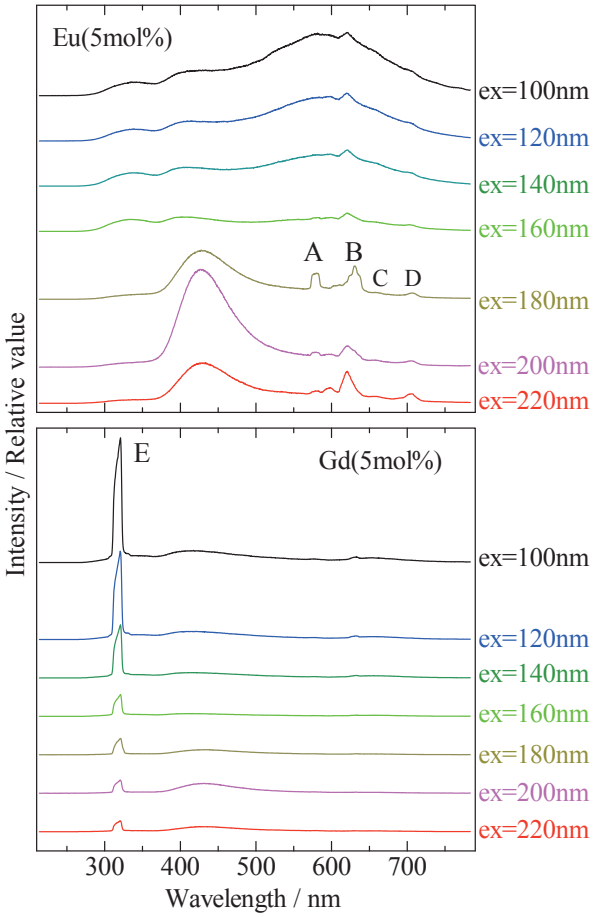

Fig. 1 Photoluminescent spectra of rare earth ion-doped hydroxyapatite samples excited by ultraviolet synchrotron orbital radiation light.

Eu^{3+}:
A: $^5D_0 \rightarrow {}^7F_1$, B: $^5D_0 \rightarrow {}^7F_2$
C: $^5D_0 \rightarrow {}^7F_3$, D: $^5D_0 \rightarrow {}^7F_4$
Gd^{3+}:
E: $^6P_{7/2} \rightarrow {}^8S$

BL1B

Temperature Dependence of Absorption Spectra for Pr^{3+} in $LiYF_4$

S. Watanabe[1], H. Kai[1], H. Yoshida[1,2], K. Ogasawara[1]

[1]*Department of Chemistry, Kwansei Gakuin University, 2-1 Gakuen, Sanda 669-1337 Japan*

[2]*Research and Development Division, NEC Lighting, Ltd., 3-1 Nichiden, Minakuchi-cho, koka, 528-8501, Japan*

The trivalent or divalent lanthanides in crystals and glasses have drawn attentions due to their application for luminescent materials in UV and VUV regions such as tunable solid-state lasers or phosphors. In those materials, transitions between the multiplet energy levels were used. In case of trivalent praseodymium ion (Pr^{3+}) in various host crystals, the $4f^2$-$4f^15d^1$ transitions lie in UV and VUV regions. Therefore, Pr^{3+} in host crystals or glasses hold the promise of good luminescent materials in UV or VUV regions.

The excitation spectrum for Pr^{3+} in $LiYF_4$ was reported by Pieterson et al [1]. They measured the excitation spectrum at 6 K using the DESY synchrotron facility. According to their report, 3 main peaks and 2 sub-peaks were observed in the excitation spectrum.

In this report, we have investigated the temperature dependence of absorption spectra for Pr^{3+} in $LiYF_4$. And we also analyzed the spectra based on the first-principles calculation for multiplet energy and absorption spectrum using the 4-component relativistic configuration interaction (CI) method [2]. This calculation method has been successfully applied to calculation of the multiplet energy levels and optical absorption spectrum between multiples for impurity ions in host crystals [3]. By measurements of the absorption spectrum at low temperature, we could directly compare the theoretical absorption spectrum to that obtained by the first-principles calculation. Therefore, the combination of measurements of the absorption spectrum at low temperature and first-principles calculations is very effective procedure for analysis of optical properties.

The $LiYF_4$ single crystal doped with Pr^{3+} were grown by Bridgeman-Stockbarger method. The concentration of Pr^{3+} ion in the sample was 0.3 mol%.

Fig. 1 shows the temperature dependence of absorption spectra for Pr^{3+} in $LiYF_4$. The absorption spectra were measured at 10, 50, 100, 150, 200 and 300 K. The 3 main peaks, A, B, C, were observed in each spectrum at 5.8, 6.7 and 7.6 eV. The first-principles relativistic CI calculation indicates that the splitting of those 3 peaks A, B, C is due to the crystal field splitting of Pr-5*d* levels. On the other hand, the 2 sub-peaks, A', B', were observed in spectrum at 10, 50, 100 and 150 K at about 6.0 and 7.2 eV. The first-principles relativistic calculation indicates that the splitting between peak A and A' and that between peak B and B' are due to the spin-orbit interaction of Pr-4*f* levels. These splittings are observed only in the spectra measured at low temperature measurements. We should point out that observation of peaks A' and B' originating form spin-orbit interaction also significantly depend on the Pr^{3+} concentration.

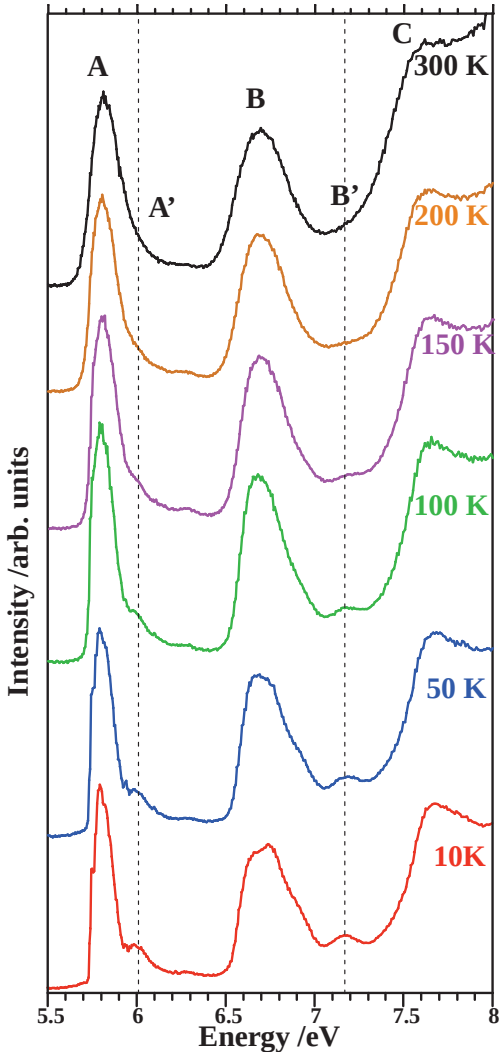

Fig. 1 The temperature dependence of absorption spectra for Pr^{3+} in $LiYF_4$. The concentration of Pr^{3+} ion is 0.3 mol%.

[1] L. van Pieterson, M. F. Reid, R. T. Wegh, S. Soverna and A. Meijerink, Phys. Rev. **B65** (2002) 045113.

[2] K. Ogasawara, T. Iwata, Y. Koyama, T. Ishii, I. Tanaka and H. Adachi, Phys. Rev. **B64** (2001) 143.

[3] K. Ogasawara, S. Watanabe, H. Toyoshima, T. Ishii, M. G. Brik, H. Ikeno and I Tanaka, J. Sol.Stat.Chem. **178** (2005) 412

BL1B

Optical Spectroscopy of Ce-doped Oxides

Y. Ohsumi, M. Yoshida, T. Hasegawa, M. Yamaga,
Faculty of Engineering, Gifu University, Gifu 501-1193 Japan

Ce^{3+}-doped crystals are attractive for applications to lasers, scintillators, and phosphors. The 4f ↔ 5d transitions of Ce^{3+} are parity- and spin-allowed so that the transition probabilities are very large. The lifetimes of Ce^{3+} in crystals are in the range of 10-60 ns [1-3]. Recently, Lu_2SiO_5 (LSO) doped with Ce^{3+} was developed as a new scintillator with high conversion efficiency from high energy to visible light. However, when there are deficits in the crystal, the emission efficiency is degraded. In addition, the afterglow is observed. This report describes optical spectra of LSO and $CaYAl_3O_7$ (CYAM) single crystals doped with Ce^{3+}, which were grown using the Czochralski method.

Figure 1 shows the vacuum ultraviolet (VUV) and UV absorption/excitation and visible fluorescence spectra in CYAM:Ce^{3+} and LSO:Ce^{3+} crystals. The optical absorption spectra of Ce^{3+} consist of five broadbands due to the transitions from the 4f ground state to the five 5d excited states. However, the absorption spectra could not be resolved because of strong absorption coefficient. Although CYAM and LSO have different crystal structure, the peak wavelengths of the fluorescence bands are about 440 nm. These fluorescence spectra have large Stokes shift. On the other hand, both excitation spectra consist of two groups: one is in the range of 200-400 nm and the other is in the range of 100-200 nm. The former corresponds to the five absorption bands of Ce^{3+}, whereas the latter may be due to band-to-band transitions with band edges around 200 nm.

The decay curves of the Ce^{3+} fluorescence in CYAM and LSO fit single exponential curves with lifetimes of about 40 ns. However, the fluorescence spectra have background intensities, which are drastically enhanced with an increase of temperature. This is called as afterglow.

Figure 2 shows the decay curve of the long-lasting phosphorescence in CYAM:Ce^{3+} at 300 K in the time range of 1-300 s in log-log scales. The decay curve does not fit a single exponential curve, but a function of t^{-n} ($n \approx 1$). In order to examine a radiative process of the phosphorescence, it is very useful to measure the excitation spectra of the phosphorescence in the VUV region. The excitation spectra for CYAM and LSO have peaks around 200 nm as the same as those of the fluorescence in Fig.1. The wavelength of 200 nm in Fig. 1 is corresponding to the band edge energy. This result suggests that electron-hole pairs produced by VUV/UV light are trapped at deficits in the crystals, such as color centers, and recombine radiatively when temperature is elevated up to room temperature.

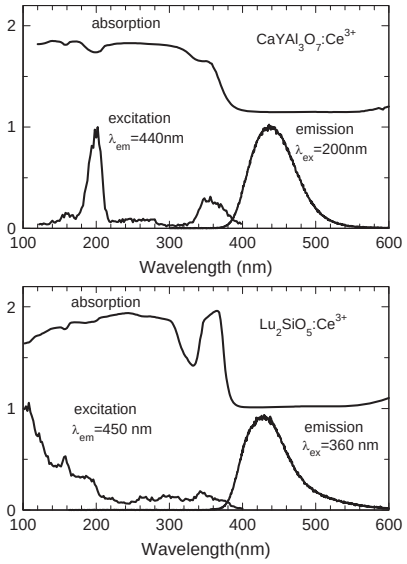

Fig. 1. Absorption, excitation and emission spectra in $CaYAl_3O_7:Ce^{3+}$ and $Lu_2SiO_5:Ce^{3+}$ measured at 17K.

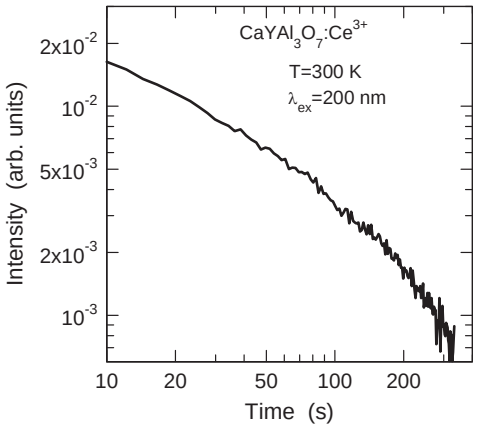

Fig. 2. Decay curve of the phosphorescence in $CaYAl_3O_7:Ce^{3+}$ measured at 300 K.

[1] E. Hayashi, K. Ito, S. Yabashi, M. Yamaga, N. Kodama, S. Ono, N. Sarukura, J. Lumin. **119-120** (2006) 67.
[2] E. Hayashi, K. Ito, S. Yabashi, M. Yamaga, N. Kodama, S. Ono, N. Sarukura, J. Alloys and Compounds **408-412** (2006) 883.
[3] M. Yamaga, E. Hayashi, N. Kodama, K. Itoh, S. Yabashi, Y. Masui, S. Ono, N. Sarukura, T.P.J. Han, H.G. Gallagher, J. Phys. Condens. Matter **18** (2006) 6033.

BL4B, BL1A

Excitation Energy Dependence of Time Resolved Decay Curves in AlGaN Alloys

T.Sakai[1], S.Suzuki[1], N.Nakagawa[1], K.Fukui[1], S.Naoe[2], H.Miyake[3], K.Hiramatsu[3]
[1]*Research Center for Development of Far-Infrared Region, University of Fukui, Fukui910-8507, Japan*
[2]*Faculty of Engineering, Kanazawa University, Kanazawa 920-1192, Japan*
[3]*Faculty of Engineering, Mie University, Mie 514-8507, Japan*

The III-V nitride semiconductors are promising materials for visible-UV opto electronic devices, such as LEDs, LDs and photo detectors. To expand the operation wavelength of LEDs and LDs into ultraviolet (UV) regions, research efforts are being made for the growth of device quality AlGaN alloys, since their band gaps spread from 3.39eV (GaN) to 6.2 eV (AlN). However, investigations into the mechanisms of near band-edge photoluminescence (PL) in AlGaN alloys are also hardly adequate. We have been measuring PL, photoluminescence excitation (PLE) and time resolved decay (TRD) curves at the excitation energy of not only near band-gap but also high photon energy up to 1.5 keV to investigate the effects of both core electron excitation and multi-electron excitation. Since all of TRD curves can be fitted as the sum of three different single exponential components (fast, middle and slow components in the order corresponding to their lifetime), we have been considering that three components suggest the existence of three energetically adjacent decay processes. In this report, we present TRD curves and their excitation energy dependence from 30 eV to 1 keV.

$Al_xGa_{1-x}N$ (x=0.34 - 0.76) samples have been made by MOVPE method at Mie University. The thicknesses of AlGaN thin films are about 1μm on 1μm AlN single crystal films with Al_2O_3 substrates. The measurement was performed in BL4B at the time of single bunch operation. A conventional 30cm VIS-UV monochromator with liquid N_2 cooled CCD detector is used for PL measurements of all samples.

Figure 1 shows time integrated PL intensity ratios among three decay components of $Al_{0.76}Ga_{0.24}N$. Measurement temperature is 9.9 K and excitation photon energy is 85 eV. The vertical line at 5.27 eV indicates the PL peak position. Below this photon energy, the contribution of LO phonon replica bands becomes dominant relative to the main PL band. It is clear that slow component is dominant and stable in the replica band region, in other words, decay process of LO phonon replicas mainly consists of slow component. However, in the main band region, intensity ratios are continuously shifted. This probably reflects inhomogeneity of cation distribution. These behaviors are similar to those results under near band-edge excitation.

Figure 2 shows TRD curves of $Al_{0.76}Ga_{0.24}N$ at various excitation energies. Measurement temperature is 9.9 K and emission photon energy is 5.27 eV. The contribution of fast component which is shown in fig. 2 as a sharp peak at 2 ns becomes large with increasing excitation photon energy. This tendency is also observed near 1.5 keV excitation. Even though the contribution of fast component becomes large, this contribution smoothly depends on the excitation photon energy and shows no drastic changes between below and above core levels. It is probably indicated that the main effect of the high energy excitation photons is multi electron-hole pair creation effect.

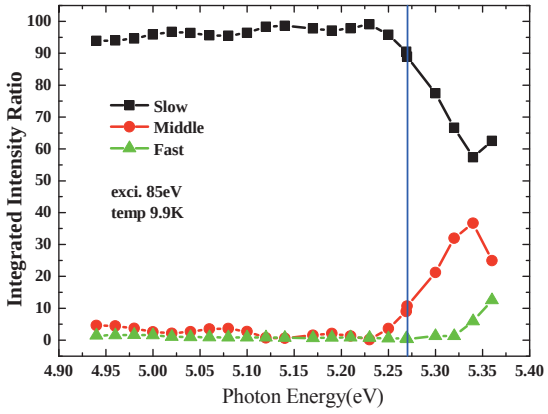

Fig. 1 Integrated intensity ratio of $Al_{0.76}Ga_{0.24}N$ at 9.9K

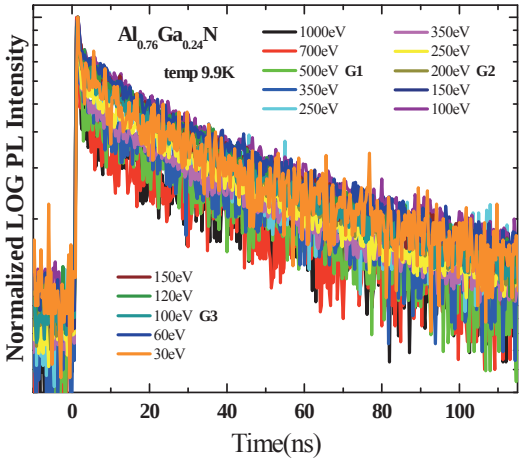

Fig.2 Time resolved decay curves of $Al_{0.76}Ga_{0.24}N$ at various excitation energies.

BL5B

Vacuum Ultraviolet Transmission Spectra of Substrate-Free Evaporated Amorphous Thin Films

K. Hayashi, K. Kimata

Department of Electrical and Electronic Engineering, Gifu University, Gifu 501-1193, Japan

Introduction

Amorphous semiconductor materials are very expected as a potential material for optoelectronic devices because these materials are very sensitive to the light and show a variety of photoinduced phenomena [1-3]. For the device application, it is necessary to sufficiently understand the physical property of these materials. Although a large number of studies have been done on the photoinduced phenomena of these materials, little is known about the details of these mechanisms. These phenomena were studied by exciting outer core electrons with the irradiation of light with the energy corresponding to the optical bandgap or sub-bandgap. The interest has been attracted for the change of the optical properties in the energy region of the visible light. We are interesting for the change of the optical properties in the higher energy region. To obtain a wide knowledge of the photoinduced phenomena, it is necessary to investigate to the photoinduced effects on wide energy region. In previous reports, we reported the photoinduced change at the VUV reflection spectra of the amorphous chalcogenide semiconductor films induced by bandgap light [4]. Recently, we measure the VUV transmission spectra of amorphous thin films prepared onto polymer membrane substrates [5]. In present work, we report the VUV transmission spectra of substrate-free evaporated amorphous thin films.

Until now, we have measured the transmission spectrum by using amorphous thin film which evaporated on the ultrathin polymer membrane substrate. However, there are some problems in this method. For example, the problems are effective decreases of the transmitted light intensity by the absorption of the polymer membrane and uncertainty of the thickness of the polymer membrane. The detection accuracy in the measurement becomes bad, when the transmitted light intensity decreases. And, it is not possible to obtain true transmission spectrum of the sample, when the thickness of polymer membrane can not be accurately measured. Then, we thought out the method for removing the polymer from the sample of the amorphous thin film which evaporated on the polymer membrane substrate.

Experimental

The ultrathin polymer membranes were prepared onto stainless steel metal plates in which two pinholes of the 1.0mm diameter opened. Thin films of amorphous chalcogenide semiconductor (a-As_2S_3 and a-As_2Se_3) were prepared onto the ultrathin polymer membranes by conventional evaporation technique. The removal of the polymer membrane tried two kinds of methods of a thermal method and a method by organic solvent. The measurement of the VUV transmission spectra were carried out at room temperature at the BL5B beam line of the UVSOR facility of the Institute for Molecular Science. And the spectrum was measured by using the silicon photodiode as a detector. To eliminate the higher order light from the monochromator, an aluminum thin film was inserted between the monochromator and sample.

Results and Discussion

Figure 1 shows the spectra of the incident light (without polymer) and the transmitted light of the polymer membrane (with polymer). As shown in the figure, the intensity of the incident light decreases under the half by the polymer membrane. Therefore, it seems to be possible to obtain the two times the signal intensity by removing the polymer membrane. Actually, it was possible to obtain the result along the expectation.

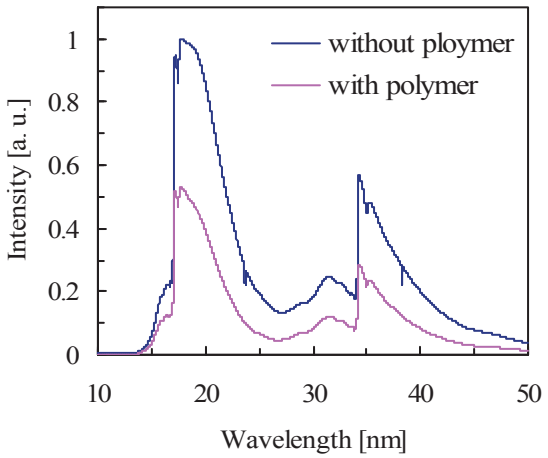

Fig. 1 Spectra of the incident light (without polymer) and the transmitted light of the polymer membrane (with polymer).

[1] Ke. Tanaka, Rev. Solid State Sci. **4** (1990) 641.
[2] K. Shimakawa, A.Kolobov, and S. R. Elliott, Adv. Phys., **44** (1995) 475.
[3] Ke. Tanaka, Encyclopedia of Nanoscience and Nanotechnology, **7** (2004) 629.
[4] K. Hayashi, UVSOR Activity Report **2001** (2002) 126.
[5] K. Hayashi, UVSOR Activity Report **2004** (2005) 79.

BL6B&7B

Optical Response of a New Type of $CaRh_2O_4$ & $NaRh_2O_4$

T.Iizuka, K.Iizuka,A.Irisawa, T.Nanba, [1]K.Yamaura
Kobe University, nada-ku, Kobe 657-8501, Japan
[1] National Research Institute for Metals, 1-2-1 Sengen, Tsukuba, 305-0047, Japan

Introduction

Recently, $CaRh_2O_4$ & $NaRh_2O_4$ have been newly synthesized by a high-pressure method in Tsukuba [1]. The oxides crystallize in a $CaFe_2O_4$-type structure. The recent electrical resistivity experiment revealed that at atmospheric pressure, $NaRh_2O_4$ exhibits a metallic property ($Rh^{3.5+}$;$Rh^{4+}(t_{2g}^5)$ and Rh^{3+} (t_{2g}^6)) but $CaRh_2O_4$ is an insulating and non-magnetic material (Rh^{3+};t_{2g}^6). Up to now, there exist no optical study except macroscopic studies such as specific heat and electrical resistivity. To study its fundamental electronic states close to the Fermi level at ambient pressure, we measured the temperature dependence of optical reflectivity spectra $R(\omega)$ of $NaRh_2O_4$ & $CaRh_2O_4$.

Experimental

The optical reflectivity spectra $R(\omega)$ at ambient pressure were measured in the wide photon energy range from 7 meV to 30 eV in the temperature range of 8-300 K. The measurements were performed using a Fourier-transform interferometer combined with a thermal light source and synchrotron radiation source at the beam line BL6B & 7B of UVSOR. The optical conductivity $\sigma_1(\omega)$and complex dielectric function $\varepsilon_1(\omega)$ were obtained from a standard Kramers-Kronig (K-K) transformation of the measured reflectivity(R) spectrum.

Results and Discussions

Fig.1 shows the temperature dependence of the R-spectra of $NaRh_2O_4$. The spectra in the low energy region exhibit a strong Drude component due to the free conduction electrons which grows with cooling. The peaks at 2.6, 6.0 and 15 and 20 eV from a visible to vacuum ultraviolet originate to the electronic interband transition.

Fig.2 shows the temperature dependence of the R-spectra of $CaRh_2O_4$.The whole spectra exhibits an insulating property. In the low energy part of the R-spectra, twelve distinct peaks were resolved which correspond to the phonon bands. They have a very weak temperature dependence. The structure in the higher energy region corresponds to the electronic interband transitions of which spectral profile is similar with $NaRh_2O_4$ but shows an additional fine structure superposed on the main peaks. Such fine structure might result from the super lattice structure due to the charge ordering states between $Rh^{4+}(t_{2g}^5)$ and Rh^{3+} (t_{2g}^6). The analysis is now on progress.

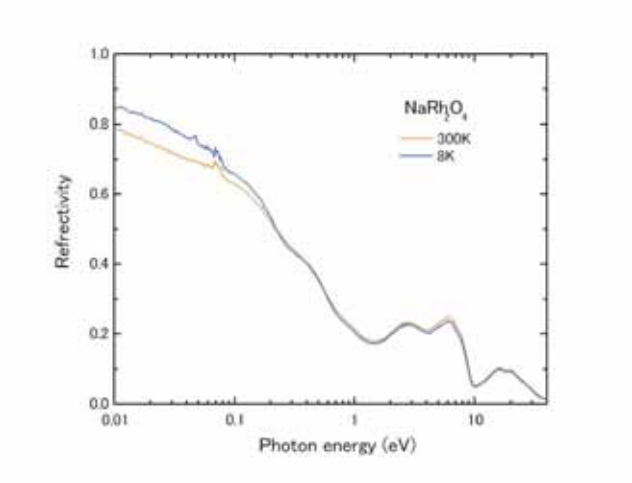

Fig.1 Temperature dependence of R-spectra of $NaRh_2O_4$ at 300 & 8 K.

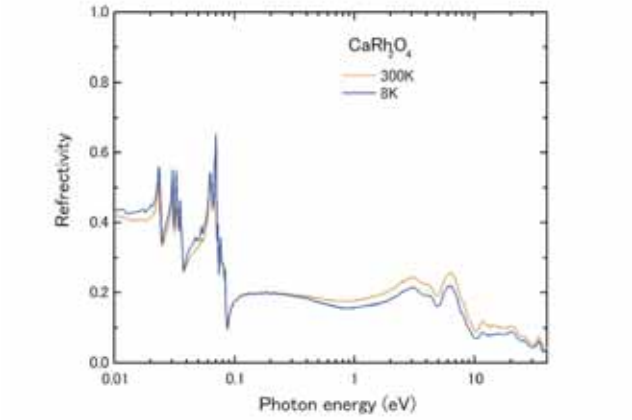

Fig.2 Temperature dependence of R-spectra of $CaRh_2O_4$ at 300 & 8 K.

[1] K.Yamaura *et al.,* Chem.Mater. **17** (2005) 359.

BL6B

Far-infrared Spectroscopy of Iodides Doped Silver Phosphate Superionic Conducting Glasses

T. Awano

Department of Electronic Engineering, Tohoku Gakuin University, Tagajo 985-8537, Japan

Enhancement of ionic conductivity by doping of PbI_2 in $AgPO_3$ glass was reported previously. Swenson et al. investigated mechanism of the enhancement on the PbI_2-$AgPO_3$ glass by diffraction measurements and reverse Monte Carlo simulation[1]. They explained the increase of ionic conductivity by that the doped Pb^{2+} substitute Ag^+ which was connected with non-bonding oxygen and the released Ag^+ contribute to ionic conduction.

The enhancement of ionic conductivity by metal iodide doping has also been reported on BiI_3, CdI_2 and other metal iodides[2]. The increase of ionic conductivity is proportional to dopant concentration and valence number of the metal ion. This abstract reports results of far-infrared spectra of high-density metal iodides doped silver phosphate glasses to investigate correlation effect of released silver ion on the enhancement of ionic conductivity, besides the above mentioned model.

Fig. 1 shows absorption spectra obtained by Kramers-Kronig analysis from the reflectivity spectra of $(AgI)_{0.5}(AgPO_3)_{0.5}$, $(BiI_3)_{0.03}(AgPO_3)_{0.97}$ and $(CdI_2)_{0.1}(AgPO_3)_{0.9}$ glasses. As previously reported, Ag-O vibration absorption in $AgPO_3$ glass is observed at 135cm^{-1}. In iodides doped glasses, it was observed at different position with different band strength. In $(CdI_2)_{0.1}(AgPO_3)_{0.9}$, the peak was at 128 cm^{-1} and shift slightly toward low wave number. In $(BiI_3)_{0.03}(AgPO_3)_{0.97}$, the strength is more than that in $(CdI_2)_{0.1}(AgPO_3)_{0.9}$ as shown in fig. 1. In $(AgI)_{0.5}(AgPO_3)_{0.5}$, the peak was at 115 cm^{-1} which is rather lower than that in $AgPO_3$.

In the above mentioned model of structural change of the glass, the number of the released silver ions is proportional to the dopant concentration and also the valence number of the doped metal ion. Therefore intensities of newly induced absorption band by Ag-I is expected to proportional to the product of the dopant concentration and the valence number. On the other hand, intensities of newly induced absorption band by Cd- or Bi-O is expected to proportional only to the dopant concentration. The intensity of Ag-O vibration should also decrease with the product of the dopant concentration and the valence number. The simulation curves in fig. 1 shows the sum of each Gaussian component of Ag-O, Ag-I and Cd- or Bi-O vibration, which are centered at 135, 100 and 165 cm^{-1}[3]. The intensity of each band is added or subtracted as above mentioned. Net absorption spectra by these component bands are shown by dashed lines in fig. 1. These simulation spectra well agree with the observed one.

The far-infrared spectral change showed the mechanism of the enhancement of ionic conductivity in iodides doped silver phosphate glasses. A doped metal ion substitutes a silver ion which is connected with a non-bonding oxygen. The released silver ion is coordinated weakly with an iodine ion and conducts easily. This mechanism is the same as that in PbI_2-$AgPO_3$ glass. The correlation effect seems to exist in lower wave number region.

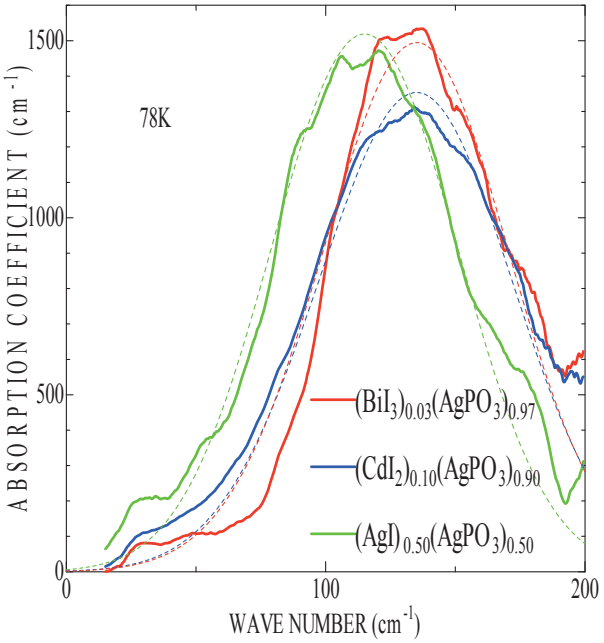

Fig. 1. Absorption spectra of iodides doped silver phosphate glasses. Absorption coefficients were obtained from reflectivity spectra by K-K transformation. Simulation curves (thin lines) by Gaussian components of Ag-I, Ag-O and Bi- or Cd-O vibration were drawn as described in the text.

[1] J. Swenson, A. Matic, C. Gejke, L. Boerjesson, W. S. Howells and M. J. Capitan, Phys. Rev. B **60** (1999) 12023.

[2] H. Takahashi, H. Nakanii and T. Sakuma, Solid State Ionics **176** (2005) 1067.

[3] B. N. Nelson and G. J. Exarhos, J. Chem. Phys. **71** (1979) 2739.

BL6B

Terahertz Spectroscopy of SmS under Pressures

T. Mizuno[1], S. Kimura[2,1], K. Matsubayashi[3], K. Imura[3], H.S. Suzuki[4], N.K. Sato[3]
[1]*School of Physical Sciences, The Graduate University for Advanced Studies (SOKENDAI), Okazaki 444-8585, Japan*
[2]*UVSOR Facility, Institute for Molecular Science, Okazaki 444-8585, Japan*
[3] *Department of Physics, Nagoya University Nagoya 464-8602, Japan*
4 National Institute for Materials Science, Tsukuba 305-0047, Japan

Introduction

SmS is a strongly correlated insulator (namely "black phase") with the gap size of 1000 K at ambient pressure.[1] Above about 0.7 GPa, the sample color changes to golden-yellow (golden phase) and the Sm-ion changes from the divalence to mixed valence.[2] To investigate the mechanism of the black-golden phase transition, we developed the terahertz (THz) reflection spectroscopic method under pressures and applied to this material.

Experimental

The THz reflection spectroscopy under pressures was performed at the THz microspectroscopy end station of BL6B. A membrane-type diamond anvil cell was employed to produce high pressures to samples. The pressure applied to samples is controlled by the helium gas pressure filled in the membrane. Since the areas of the culet plane of diamond and of the membrane are 1.13 mm^2 and 10^3 mm^2, respectively, the pressure of samples is about 10^3 times larger than the helium gas pressure. The sample with a typical size of 0.4×0.4×0.05 mm^3 was set in a diamond anvil cell with Apiezon-N grease as the pressure medium and with a gold film as a reference and ruby tips as for a pressure reference. The pressure was calibrated by a ruby fluorescence measurement.

Results and Discussion

The obtained reflectivity spectrum [$R(\omega)$] of SmS at 300 K as a function of pressure are shown by thick lines in Fig. 1(a). At the ambient pressure, the spectrum indicates the insulating character because the low energy limit does not approach to unity and a clear large peak due to the TO-phonon between Sm^{2+} and S^{2-} ions appears. When pressures were applied, the background intensity increases with increasing pressure. The background that originates from the Drude component indicates the existence of carriers. Therefore the carrier density increases with increasing pressure. The fitting curve of the combination of a Drude and a Lorentz functions is shown by thin solid lines in the same figure. The Lorentz function was set to reproduce the TO-phonon absorption. To fit the obtained spectra, the N_{eff} in the Drude function is only changed and the other parameters (the relaxation time in the Drude function and all parameters in the Lorentz function) are fixed. The obtained N_{eff} is plotted in Fig. 1(b). The logN_{eff} is proportional to the pressure up to 0.65 GPa. The pressure dependence indicates that the energy gap closes with increasing pressure. The energy gap size (2Δ) at the ambient pressure was evaluated to be about 1000 K [3]. By evaluating the gap size from N_{eff}, the energy gap at the black-golden phase boundary is 850 K and then the gap suddenly closes to 100 K in the golden phase by the first order transition. This result indicates that the charge instability occurs at the phase boundary with the gap size of 850 K.

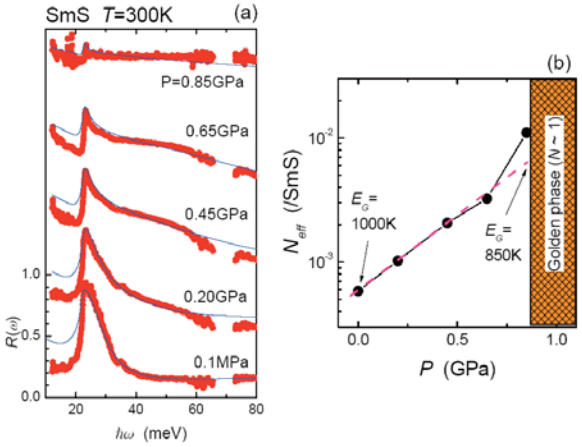

Fig.1. (a) Pressure dependence of reflectivity spectrum [$R(\omega)$] of SmS (thick lines) in the black phase at 300 K. The fitting curve of the combination of a Drude and a Lorentz functions are also plotted by thin solid lines. Successive curves are offset by 0.5 for clarity. (b) Pressure dependence of energy gap evaluated by the Drude and Lorentz fitting of $R(\omega)$ spectra.

[1] K. Matsubayashi, K. Imura, H.S. Suzuki, T. Mizuno, S. Kimura, T. Nishioka, K. Kodama, and N.K. Sato, J. Phys. Soc. Jpn. (2007) in press.
[2] J.L. Kirk, K. Vedam, V. Narayanamurti, A. Jayaraman, and E. Bucher, Phys. Rev. B **6** (1972) 3023.
[3] T. Mizuno, S. Kimura, K. Matsubayashi, K. Imura, H.S. Suzuki, and N.K. Sato, submitted.

BL6B(IR)

Dielectric Spectroscopy of $Ba_4R_{9.33}Ti_{18}O_{54}$ (R=La and Sm) Ceramics

K. Wada, Y. Yamada, I. Kagomiya, K. Kakimoto, H. Ohsato
Graduate School of Engineering, Nagoya Institute of Technology, Gokiso-cho, Showa-ku, Nagoya 466-8555 Japan

$Ba_4R_{9.33}Ti_{18}O_{54}$ is a paraelectric material with tungsten-bronze-like crystal structure. Characteristics of $Ba_4R_{9.33}Ti_{18}O_{54}$-based material with both high permittivity (ε_r) and the temperature stability at GHz frequency range are proper to a resonator or filter application for the wireless telecommunication devices. In general, temperature coefficient of permittivity (τ_ε) of high-permittivity paraelectric material shows large negative value, e.g. $SrTiO_3$ (ε_r = 304, $\tau_\varepsilon \approx$ -3200 ppm/°C), $CaTiO_3$ (ε_r = 162, $\tau_\varepsilon \approx$ -1700 ppm/°C) and TiO_2 (ε_r = 104, $\tau_\varepsilon \approx$ -900 ppm/°C). On the other hand, the τ_ε of $Ba_4R_{9.33}Ti_{18}O_{54}$ strongly depends on the R species in spite of the crystal symmetry retention. $Ba_4La_{9.33}Ti_{18}O_{54}$ (ε_r = 114; BLaT) shows τ_ε of about -800 ppm/°C whereas $Ba_4Sm_{9.33}Ti_{18}O_{54}$ (ε_r = 78; BSmT) demonstrates τ_ε of almost zero. Understanding of this difference is not sufficient despite much investigation for the development of dielectric property has been performed.

IR reflectivity spectra give us useful information, i.e. the lattice vibration, which essentially correlates to the dielectric behavior at high frequency. Dielectric spectroscopy at the frequency range from sub-millimeter to THz can be obtained by the analysis of IR reflectivity. In this study, we measured the reflectivity spectra of BLaT and BSmT to examine the dielectricity of $Ba_4R_{9.33}Ti_{18}O_{54}$.

Reflectivity spectra of BLaT and BSmT dense ceramics were obtained in the temperature range of 10-300 K at the BL6B beam line of UVSOR. The spectra below 150 cm^{-1} were corrected by Martin-Puplett interferometer (JASCO, FARIS-1) and synchrotron radiation source. Measurement at higher frequency range (>150 cm^{-1}) was carried out using Michelson interferometer (Bruker, IFS66v) and glow-bar source. Each peak of the imaginary part of dielectric spectroscopy obtained from Kramers-Kronig transformation of experimental spectra was used as an initial parameter (TO mode) for the fitting. Then, the experimental spectra were fitted by Drude-Lorentz model.

Fig.1 shows far-infrared reflectivity spectra (circle) and their fits (solid line) of BLaT and BSmT at 300 and 10 K, respectively. Observed spectra are similar to that of Pr-analogy reported in the literature [1]. The portion of the spectra above 1000 cm^{-1} is not shown since no reflection bands were observed. Because of the complexity of the crystal structure in BLaT and BSmT, the spectra showed much dip resulted from the many vibration modes. From the factor group analysis based on the crystal structure data, BLaT and BSmT have 203 IR active modes. Actually, fitting was carried out by use of less than 30 modes because small number of strong modes and/or bundled modes can represent the dielectric behavior approximately. The fitted spectra are good agreements with the observed ones. Usually, low-frequency modes in high-permittivity paraelectric material show softening toward to the Currie temperature. However, in this study, the softening was not confirmed for the less change in the spectra of BLaT and BSmT. The lack of distinct changes in the spectra suggests that no ferroelectric phase transition occurs in both materials at least down to 10 K. Fig. 2 shows real part of permittivity obtained from the fitting of spectra of BLaT. Although BLaT shows large temperature dependence of permittivity below at several GHz ranges [2], the permittivity obtained from IR reflectivity exhibits small temperature dependence. These phenomena can be well connected if BLaT has broad dielectric dispersion. Therefore, $Ba_4R_{9.33}Ti_{18}O_{54}$ probably belongs not to normal paraelectrics but to relaxor dielectrics with broad dielectric dispersion.

[1] K. Fukuda, R. Kitoh and I. Awai, J. Mater. Sci. **30** (1995) 1209.
[2] A. Belous, O. Ovchar, M. Valant and D. Suvorov, J. Appl. Phys. **92** (2002) 3917.

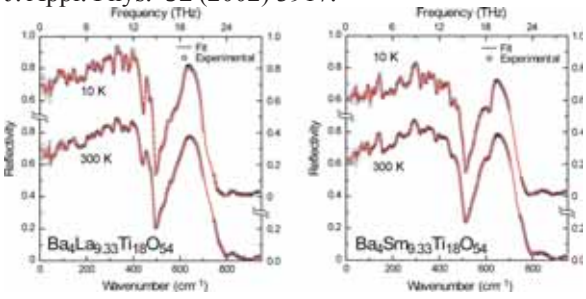

Fig. 1. Far-infrared reflectivity spectra together with their fits of $Ba_4La_{9.33}Ti_{18}O_{54}$ and $Ba_4Sm_{9.33}Ti_{18}O_{54}$ ceramics at 10 and 300 K.

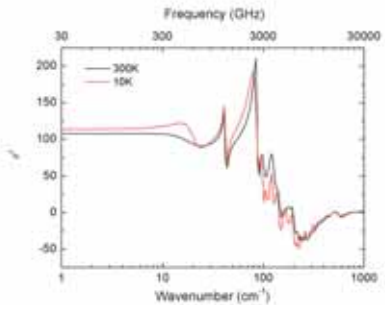

BL6B(IR)

Optical Properties of Bismuth Clusters

S. Yoshida, A. Goyo, H. Ikemoto
Faculty of Science, University of Toyama, Gofuku 3190, Toyama 930-8555, Japan

It is well known that small clusters of atoms will have a local structure and a property different from their elemental crystalline equilibrium.

Raman-scattaring measurements of cluster of Bi exhibit phase transition from rhomdohedral Bi nanocrystalline to amorphouselike clusters depending on cluster size[1]. They also suggest that amorphous clusters are semiconducting and covalent interactions increase with decreasing size.

The Raman studies are good tools but indirect evidences for the transition. So it is very important to investigate the optical property directly to reveal the mechanism of the phase transition. In the present study we report results of optical absorption coefficients for Bi clusters.

Experimental

Bismuth of 99.999 % purity was slowly deposited onto the substrates from a melting crucible. The Bi film was discontinuous with isolated island formation. Then, KBr of 99.99 % purity was deposited to cover the Bi islands. By repeating these procedures, a sample of Bi clusters isolated in a KBr matrix was obtained. The size of the islands was adjusted by controlling the thickness deposited on the substrates, which was monitored with a quartz oscillator. The thickness ratio of the Bi and the matrix is about 1:20. As mentioned above the Bi clusters are formed in thin films, and samples are represented by their average thickness of the Bi thin films in this paper. The measurements of reflectivity and transmissivity were performed in the energy range of 0.05~0.8 eV with the rapid-scan Michelson interferometer (Bruker, IFS-66v) and a HgCdTe detector at the UVSOR. All measurements were performed at room temperature.

Results and Discussion

Figure 1 shows the measured transmittance spectra of the Bi 10nm thick films with comparison with those calculated by two models. In a multilayer(ML) model the layers of Bi and KBr are assumed to be uniform respectively. In an effective medium(EM) model it is assumed that there is a single layer composed of mixture of Bi clusters and KBr matrix, and optical constants of the layer are mixed optical constants of Bi[2] and those of KBr[3] are mixed in the ratio of the thickness. The EM model is better than that the ML models for 10nm thick films.

The absorption coefficients are calculated by Hong's expression[4]. The absorption coefficients of 10nm thick films are close to those of crystalline Bi, suggesting that 10nm thick films are semimetal. Meanwhile the absorption coefficients of the 2nm and 0.5nm thick films are smaller than those of bulk Bi. These results suggest the semimetal-semiconductor transition of Bi clusters.

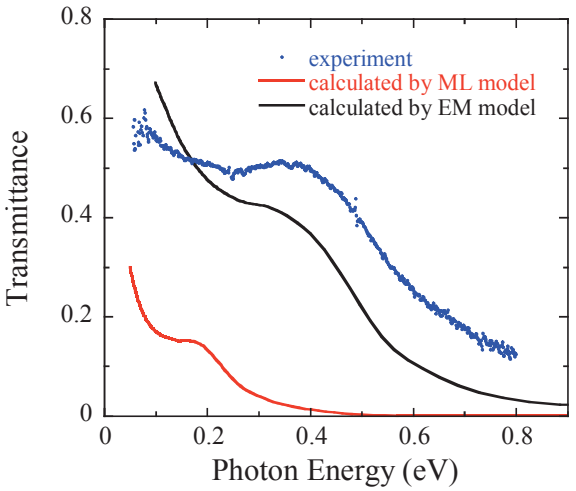

Fig. 1. Transmittance of the 10 nm-thick films. Measured transmittance (blue), transmittances calculated by ML models(black) and EM model(red).

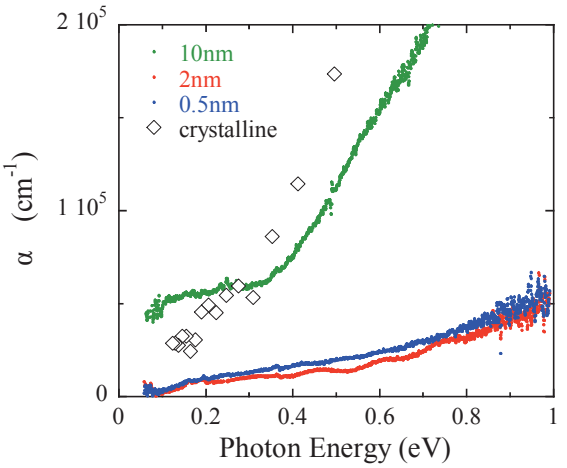

Fig. 2. Variations in optical absorption coefficients of the as-deposited Bi clusters for different thickness. Open circles denote those of polycrystalline [2].

[1] M. G. Mitch, S.J.Chase, J Fortner, R.Q. Yu, and J. S. Lannin, Phys. Rev. Lett. **67** (1991) 875-878.
[2] A.D.Lenham,et al. J.Opt.Soc.Am.**55** (1965) 1072.
[3] Handbook of optical constants of solids II. Academic Press (1991).
[4] W.Q.Hong, J.Phys.D:Appl.Phys.**22**(1989)1384.

BL6B

Infrared Reflection Absorption Spectroscopy of Potassium Doped Alq_3 Thin Film Using Synchrotron Radiation

Y. Sakurai[1], S. Kimura[1,2], K. Seki[3]

[1]*UVSOR Facility, Institute for Molecular Science, Okazaki 444-8585 Japan*

[2]*School of Physical Sciences, Graduate University for Advanced Studies, Okazaki 444-8585 Japan*

[3]*Department of Chemistry, Graduate School of Science, Nagoya University, 464-8602 Japan*

Tris-(8-hydroxyquinoline) aluminum (Alq_3) (figure 1) is most widely used as the electron transport/light emitting layer in organic light emitting diodes (OLEDs). A typical OLED consists of indium tin oxide (ITO) as the anode on which organic thin films are sequentially deposited, with low work function metals finally deposited as the cathode. The property of the interface between cathode metals and Alq_3 affect the performance of the devices. Doping is on way to modify the electronic property of the interface.

Infrared reflection absorption spectroscopy (IRAS) is a powerful probe for the structure and chemistry of a surface and interface. Al-N and Al-O vibrational modes of Alq_3 which are expected to be significantly affected by alkali metals appear in the wavenumber region lower than 600 cm^{-1}. Since a conventional FTIR system using a globar light source cannot cover the wavenumber region because of its low brilliance, we have performed IRAS measurement of potassium doped Alq_3 thin film using a high brilliant synchrotron radiation, UVSOR-II, in the region between 300 and 500 cm^{-1}. The change of the Al-N stretching mode with the potassium doping was observed [1]. In this study, we measured IRAS spectra in the region between 400 and 700 cm^{-1} to observe Al-N and Al-O stretching modes.

Experiments including the sample preparation and measurement were performed in an ultrahigh vacuum chamber specially designed for this experiment [2]. Alq_3 films were prepared by vacuum evaporation onto Ag films deposited on Si substrates. Potassium was evaporated on the Alq_3 films from SAES getter sources. IRAS spectra were obtained with the SR light through CsI windows at the incident angle of 80° relative to the surface normal. The reflected light was detected by a liquid-helium-cooled Si bolometer.

Figure 2 shows the potassium doping dependence of the IRAS spectra of an Alq_3 film of 20 nm thickness in the wavenumber region between 400 and 700 cm^{-1}. In the pristine Alq_3 spectrum, four strong peaks at 422, 458, 552 and 655 cm^{-1} are observed. These peaks are assigned to Al-N stretching, pyramidalization modes of the nitrogen atom, Al-O stretching and pyramidalization modes, respectively, as previously assigned by absorption spectra of powder Alq_3 samples [3]. The intensity of these peaks gradually decreases and new peaks additionally appeare around 440 and 502 cm^{-1} with increasing potassium evaporation amount. These new peaks are assigned to Al-N and Al-O stretching modes, respectively, by comparing with calculated vibrational modes. Therefore the frequency of Al-N stretching mode changed to higher frequency, and that of Al-O stretching mode changed to lower frequency, i.e., the Al-N bond strengthens and the Al-O bond weakens by the potassium doping. These changes are believed to be caused by the charge transfer from the potassium atom to the Alq_3 molecule which is predicted by theoretical investigation.

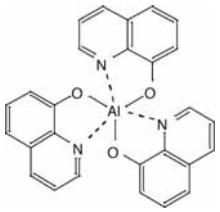

Fig. 1 The chemical structure of Alq_3.

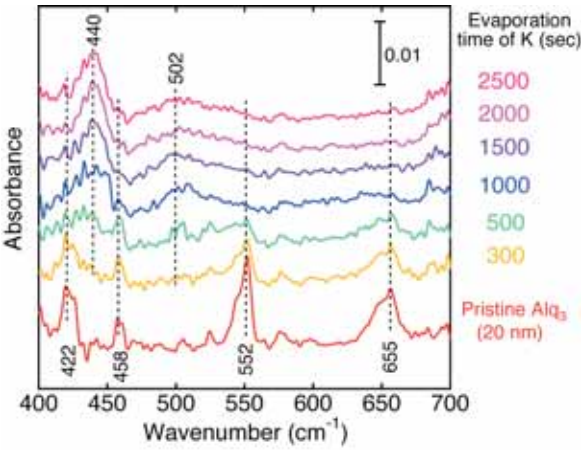

Fig. 2 The potassium doping dependence of the IRAS spectra of an Alq_3 film.

[1] Y. Sakurai, S. Kimura and K. Seki, UVSOR Activity Report 2005 (2006) 81.

[2] S. Kimura, Y. Sakurai, E. Nakamura and T. Mizuno, AIP Conf. Proc. **879** (2007) 595.

[3] M. Cölle, S. Forero-Lenger, J. Gmeiner and W. Brütting: Phys. Chem. Chem. Phys., **5** (2003) 2958

Reflectivity of $YbAl_2$ in Visible to VUV Regions

H. Okamura[1], S. Nagano[1], T. Nanba[1], M. Kosaka[2]
[1]*Graduate School of Science and Technology, Kobe University, Kobe 657-8501, Japan.*
[2] *Department of Physics, Saitama University, Saitama, Japan.*

At ambient pressure, the average 4*f* electron configuration of Yb in $YbAl_2$ is $(4f)^{13.8}$, hence the average valence of Yb is 2.2. It has been shown that $YbAl_2$ undergoes a valence crossover under external pressure, from 2.2 at ambient pressure to nearly 3 at 16 GPa [1]. When the valence of Yb is 3+, it has a hole within the 4*f* shell; hence it possesses a localized magnetic moment. Namely, as the applied pressure is increased, the number of localized 4*f* holes increases. This can be viewed as a pressure-induced crossover from itinerant to localized character of the 4*f* electrons through the electron-hole symmetry. Associated with this crossover, there should be also changes in the strength of the hybridization between the conduction and 4f electron (*c-f* hybridization). This is an interesting system where the degree of f electron localization can be tuned continuously by the applied pressure. We are planning an infrared study of $YbAl_2$ under pressure, to explore the crossover of electronic states under pressure. To do so, it is important to measure its optical spectra in detail at ambient pressure in a wide photon energy range. As a part of this, we have carried out reflectivity measurements of $YbAl_2$ at BL7B from visible to vacuum UV regions.

Fig. 1 shows the measured reflectivity spectrum of $YbAl_2$ single crystal. It is seen that the reflectivity decreases rapidly above 2 eV, reaching a minimum (plasma edge) at 8 eV. We are also measuring the reflectivity in the infrared region, so the spectrum in the entire region can be analyzed via the Kramers-Kronig analysis to obtain the optical conductivity spectrum of $YbAl_2$.

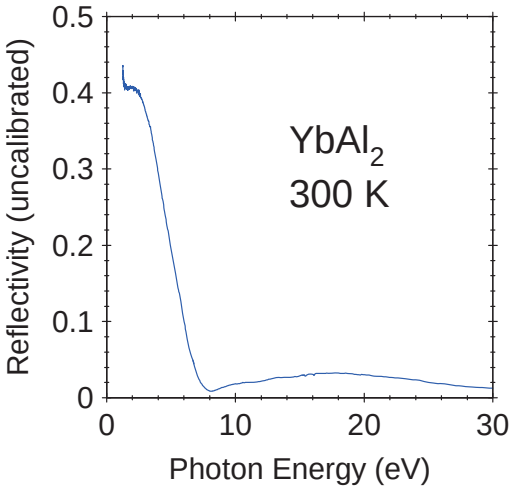

Fig. 1. Reflectivity spectrum of $YbAl_2$ at room temperature. Note that since the sample size was smaller than the SR beam spot size on the sample, the absolute value of the reflectivity is not correct (uncalibrated).

[1] C. Dallera et al., Phys. Rev. B **68** (2003) 245114.

BL7B

Reflection Spectra of Polyimide (CBDA/BAPP) Films Exposed to Polarized UV Radiation

T. Mizunuma, K. Nakagawa, T. Tsuda, S. Matsumoto
School of Science and Technology, Meiji University, Kawasaki 214-8571 Japan

Polyimides compounds based on aromatic dianhydrides and diamines are widely used as base materials for electronic devices, becouse of their thermal stability and chemical resistance. Recently it has been reported that polyimide films exposed to linearly polarized Ultraviolet (UV) radiation are capable of aligning liquid crystal(LC) molecules on their surface. This technique, named photo alignment, is remarkable for fabricating Liquid Crystal Displays (LCD's). But the detailed mechanism of photo alignment of LC molecules has not been clear. Optical spectra of polyimide films in the UV-VIS and IR regions give important clues to infer the photo alignment mechanism[1][2][3]. But few spectroscopic investigation has been made about higher energy regions such as vacuum ultraviolet (VUV) region. In this paper, we report VUV reflection spectra of polyimide (CBDA/BAPP) films exposed to linearly polarized UV radiation.

Experimental

An amic acid form of CBDA/BAPP from Nissan chemical Industries, Ltd was used and suitable concentrations of the poly (amic acid) (PAA) form was spin coated on quartz substrates. Spin condition was 3500 rpm for 40 s and film thickness was about 50 nm. They were soft baked for 10 min at 100 ^{o}C to remove the solvents and hard baked 250 ^{o}C in a convection oven to accomplish imidization for 2 hours. UV irradiation was accomplished using a He-Xe lamp based irradiator. The intensity of the UV radiation was about 5.5 mW/cm^2 around 365 nm. Reflection spectra of polyimide (CBDA/BAPP) films exposed and without exposed to linearly polarized UV radiation were measured in the vacuum ultraviolet region up to 25.0 eV with the 3-m normal incident type monochromator (grating: G1 and G2) at BL-7B of UVSOR-II.

Results and Discussion

Figure 1 shows the reflection spectra of polyimide (CBDA/BAPP) films exposed to linearly polarized UV radiation compared with that of no exposed film. Peaks in the figure are named as indicated for convenience. In the reflection spectra, five peaks named as A, B, C, D and E were observed at about 6.0 eV, 9.5 eV, 13.0 eV, 16.0eV and 20.0eV, respectively. Therefore both reflection spectra show some remarkable peaks at same energies. But peak intensities of spectrum exposed to UV radiation becomes stronger than that of without exposed except peak A. It is considered that molecular reorienteation occurred by linearly polarized UV radiation. To analysis of spectra changes caused by exposed to linearly UV radiation, DV-Xα molecular orbital calculation was performed. Figure 2 shows Density of State (DOS) spectra calculated. Peak A has been reported to π-π* transition on a benzene ring. And it is already known that n-π* transitions is dominant for alicylic polyimides, which implies the peaks B, C, D and E may be attributed to n-π* transitions of carbonyl groups contained in CBDA/BAPP as drawn in Fig 2.

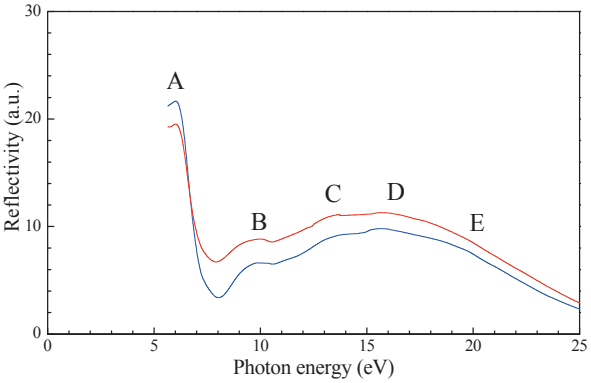

Fig. 1 Reflection spectra of polyimide (CBDA/BAPP) films exposed (red line) and without exposed (blue line) to linearly polarized UV radiation.

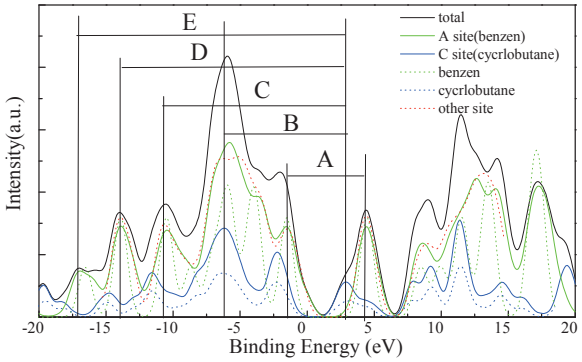

Fig. 2 DOS spectra of polyimide (CBDA/BAPP) calculated by DV-Xα method.

Acknowledgements

The authors would like to thank H. Shitomi of AIST for his support.

[1] H. Endo, T. Shinozuka, H. Fukuro, Y. Imura and S. Kobayashi, AM-LCD(1996)341.
[2] H. Shitomi, T. Ibuki, S. Matsumoto and H. Onuki, Jpn.J.Appl.Phys. **38** (1999)176.
[3] K. Sakamoto, K. Usami, T. Araya and S. Ushioda, Jpn.J.Appl.Phys. **38** (1999)1435.

Optical Investigation of the Charge Gap Opening in $FeSb_2$

M. Marutzky, S. Kimura[1], J. Sichelschmidt, A. Bentien, F. Steglich
Max-Planck Institut für Chemische Physik fester Stoffe, Dresden, Germany
[1]UVSOR Facility, Institute for Molecular Science, Okazaki 444-8585, Japan

Introduction

$FeSb_2$ is characterized as a Kondo-insulator with similar physical properties to FeSi [1, 2]. It shows a crossover from a diamagnetic to a paramagnetic state around 100 K [3, 4]. In the literature, a semiconducting behaviour for two crystal axes and a metal-semiconductor crossover for the third axis was reported [3]. We have grown single crystals and found a semiconducting behaviour for all three axis and a colossal Seebeck coefficient [2]. In order to study the correlation effects in $FeSb_2$, we started an optical investigation over a large energy range from the FIR (3meV) to the VUV (30 eV).

Experimental

Single crystals of $FeSb_2$ were grown by flux method. The optical anisotropic crystals have a large [110] surface which was polished in order to allow optical measurements with the E vector parallel and perpendicular to the c-axis. Michelson- and Martin-Puplett Fourier transform spectroscopy was used in the IR where the contribution of the conduction carriers to the optical properties can be observed. Additionally, reflectivity measurements were made from 1 to 30 eV at BL7B of the UVSOR which was necessary in order to investigate the interband transitions and to enable an exact Kramers-Kronig transformation (KKT) of the reflectivity. The latter is needed to calculate the complex optical conductivity.

Results and Discussion

In Figure 1 the reflectivity of $FeSb_2$ with $E \parallel c$ from 3 meV to 30 eV is depicted at various temperatures. At 300 K, the reflectivity in the FIR is predominant metal-like. Remarkable is the fact that at 24 meV a peak is visible arising from phonon absorption which is unusual for a metal. At 50 K, the reflectivity has changed dramatically and dropped from approx. 0.9 at 300K down to 0.7. This is similar to the situation in FeSi where a charge excitation gap opens [5]. Very distinctive phonon structures appear with a minimum reflectivity of 0.1 at 10 K. The drastic depletion of the reflectivity and the absorptive part of the optical conductivity was also observed in [6]. Qualitatively the same behaviour occurs for $E \perp c$, not shown here. A quantitative analysis of these optical spectra will help to answer the question if the intriguing physical properties of $FeSb_2$ can be understood in the framework of a Kondo model.

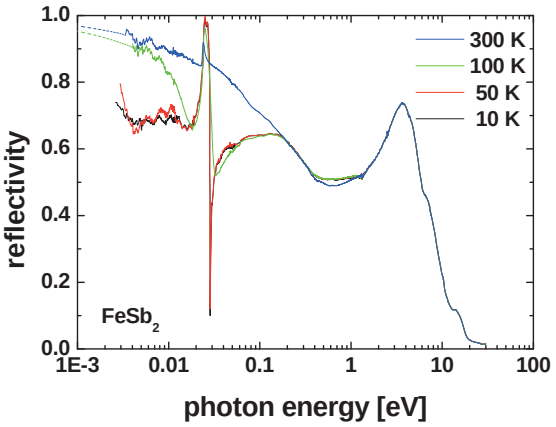

Fig. 1 Reflectivity of single crystalline $FeSb_2$ with E parallel to the c-axis in the [110] plane. For 100 and 300 K, the reflectivity was extrapolated down to zero with the Hagen-Rubens relation in order to enable a KKT. Above 30 eV, $R \sim \omega^{-4}$ was used for extrapolation.

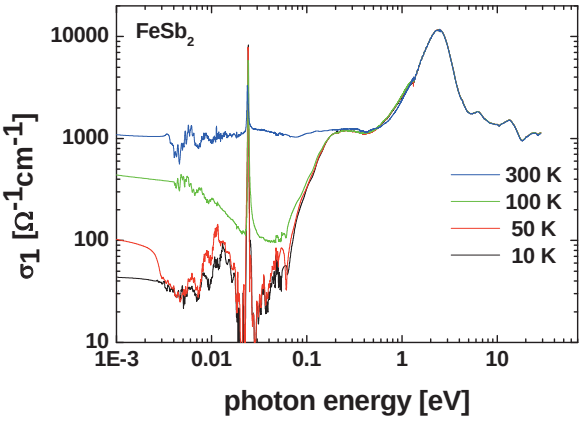

Fig.2 Real part of the optical conductivity, obtained by Kramers-Kronig transformation of the reflectivity data in Fig. 1.

[1] C. Petrovic et al., Phys. Rev. B **72** (2005) 045103.
[2] A. Bentien et al., submitted to Nature Physics
[3] C. Petrovic et al., Phys. Rev. B **67** (2003) 155205.
[4] Ronwei Hu et al., Phys. Rev B **74** (2006) 195130.
[5] Z. Schlesinger et al., Phys. Rev. Lett. **71** (1993) 1748.
[6] A. Perucchi et al, Eur. Phys. J. B **54** (2006) 175-183.

BL7B

Temperature Dependence of Time Resolved Decay Curves in AlGaN Alloys

M.Suzuki[1], T.Sakai[1], N.Nakagawa[1], K.Fukui[1], S.Naoe[2], H.Miyake[3], K.Hiramatsu[3]

[1]*Research Center for Development of Far-Infrared Region, University of Fukui, Fukui910-8507, Japan*

[2]*Faculty of Engineering, Kanazawa University, Kanazawa 920-1192, Japan*

[3]*Faculty of Engineering, Mie University, Mie 514-8507, Japan*

AlGaN alloys have a great potential for UV opt-electronic devices, because AlGaN alloys can cover their band gap energies from 3.39 to 6.2 eV by changing a compositional rate of Al and Ga. Then, to understand the decay processes of near band edge ultraviolet (UV) photo luminescence (PL) in AlGaN, we have been performing the measurement of the time resolved decay (TRD) curves of AlGaN alloys. In this report, temperature dependence of TRD curves in AlGaN alloys is presented.

All samples are made by the MOVPE method. The thicknesses of AlGaN thin films are about 1μm on 1μm AlN single crystal thin films with Al_2O_3 substrates. The all measurements were carried out at BL7B under single-bunch operations. A optical fiber is used for guiding PL in the vacuum sample chamber to a spectrometer with CCD. Time resolved decay curve measurements are carried out by using time correlated single photon counting (TCSPC) method.

Figure 1 shows TRD curves at various temperatures (from 10 to 170 K) of $Al_{0.67}Ga_{0.33}N$. Excitation energy is 5.01 eV where PL excitation spectrum becomes maximum intensity. As shown in fig. 1, these curves can not be analyzed as a single exponential decay process. We have been considering that TRD curves consist of three different single exponential decay components. Decay times of first, middle and slow components are less than 1 ns (less than resolution limit of TCSPC), order of ns ~ 10 ns, and order of 10 ns ~ 100 ns, respectively. Decay time of each component also decreases with increasing temperature as shown in fig. 1. Time integrated PL intensity of each component is calculated from the product of decay time with initial intensity, and fig. 2 shows normalized time integrated PL intensity of each component which is derived from the analyzed results of TRD curves shown in fig. 1. The curve labeled as 'total' in fig. 2, which represents simple sum of three components, is in good agreement with temperature dependence of PL intensity obtained from time integrated PL measurement at 5.01 eV. The temperature dependence of slow component indicates that the decay process corresponds to the slow component is dominant process at low temperature and this decay process basically shows temperature quenching; there are potential barriers which connect another processes, and the role of the radiative process by slow component decreases with increasing temperature. One of 'another processes' is a non-radiative process, but the temperature dependence of middle component clearly suggests that the other 'another process' is the radiative process by middle component. Similar intensity exchange is also found between middle and fast components.

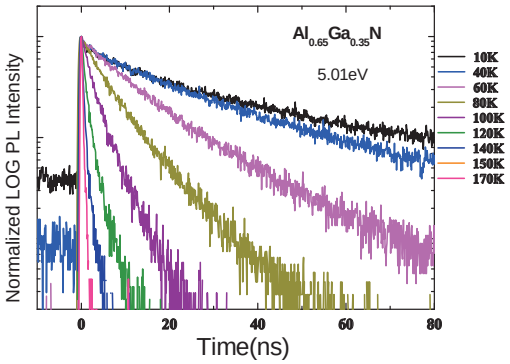

Fig.1 Time resolved decay curves of $Al_{0.67}Ga_{0.33}N$ at 5.01eV

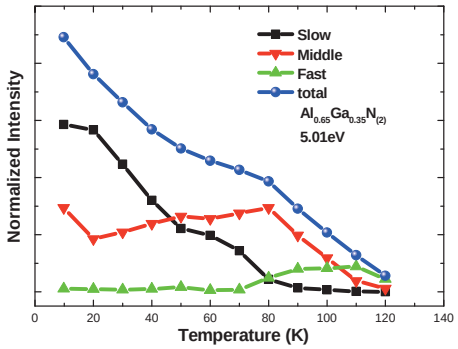

Fig.2 Temperature dependence of area strength at PL energy peak position(5.01eV)

BL7B

Angle Dependence of Polarized Reflectance Spectra in AlN

F.Suzuki[1], M.Kishida[1], K.Fukui[1]

[1]*Research Center for Development of Far-Infrared Region, University of Fukui, Fukui910-8507, Japan*

AlN has a large bandgap of about 6 eV and a high thermal resistance, and is expected in fields such as lasers and LED in the ultraviolet and the deep ultraviolet. Usually, high quality AlN single crystal is fabricated as a thin film by MOCVD method. AlN thin film has the wurtzite structure and *c*-axis is perpendicular to the surface. In this restriction, reflectance measurements are usually carried out under $\boldsymbol{E} \perp c$ condition, where $\boldsymbol{E}$ represents the electric field of incident light. In this condition, optical transition which corresponds to the minimum bandgap becomes forbidden transition due to the selection rule, and first allowed transition is observed at 6.2 eV. For this reason, the true bandgap has been reported using unobtainable bulk crystals even though crystal quality of the bulk sample is lower than that of thin film. However, it is possible to investigate optical properties around true bandgap of high quality AlN thin film by using the reflectance spectra with incidence angle dependency and high linear polarization incident light. In this report, we present angle dependence of polarized reflectance spectra in AlN by using BL7B.

High quality AlN thin film has a wurtzite structure which is evaporated on the sapphire substrate by MOVPE method. Thickness of AlN film is 1μm. Reflectance measurement at 10 K has been carried out in the range between 5.8-7eV, and the incidence angles to the surface normal are 6, 15, 30, 45, and 60 degrees.

Figure 1 shows the reflectance spectra of AlN at 6, 15, 30, 45, and 60 degrees. In all spectra, wave-like features by interference are shown in the transparance region (below 6.2eV), and the peak with dip structures due to exciton absorption are also seen near 6.2 eV. However, wave-like features become discontinuous near 6.0 eV with increasing incidence angle. This is caused by the exciton absorption at minimum bandgap, since $\boldsymbol{E}$ // c component of incident light becomes increasing with increasing incidence angle. Although band edge absorption begins at 6.0 eV by $\boldsymbol{E}$ // c component of incident light, AlN is still transparance under $\boldsymbol{E} \perp c$ condition. Then, wave-like features still exist up to 6.2 eV with its intensity decreasing.

Figure 2 shows the refractive index *n* and the extinction coefficient *k* derived from reflectance spectra shown in Fig. 1 by using the characteristic matrix of the single-layer thin film model. Clear jumps of *k* which corresponds to optical absorption can be seen in not only ~ 6.2 eV but also ~ 6.0 eV at grazing incidence conditions.

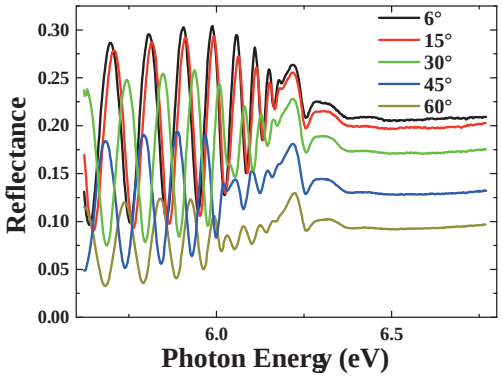

Fig. 1 Reflectance spectra of AlN of 6, 15, 30, 45, and 60 degrees

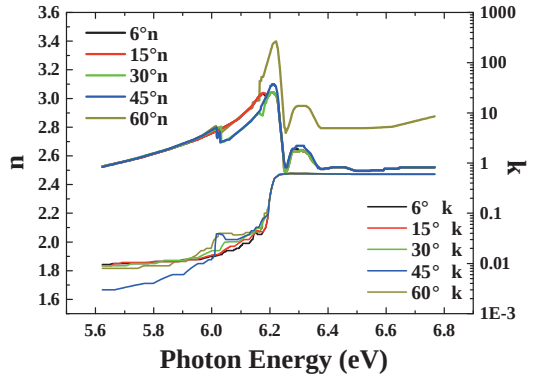

Fig. 2 Optical constant n and k to each incidence angle

BL7B

Photoluminescence of Forsterite Single Crystals Excited by Vacuum Ultraviolet Radiation

M. Kitaura[1], S.Izuhara[2], H.Nakagawa[2], A.Ohnishi[3]
[1]*Fukui National College of Technology, Sabae, 916-8507, Japan*
[2]*Dept. of Electrical and Electronics Engineering, Fukui University, Fukui, 910-8507,Japan*
[3]*Deparment of Physics, Yamagata University, yamagata, 990-8560, Japan*

Magnesium silicate (Mg_2SiO_4) is orthorhombic at normal condition, which is named forsterite. This material has been used as the host of radiation dosimeter. The application of it extends to the other optical materials, e.g., laser, phosphor and so on. Because of its industrial importance, most of the studies concentrate in optical properties of activator ions. There are few reports on optical properties of forsterite, except for our optical constant data [1]. It seems valuable to investigate the optical properties of forsterite from the viewpoint of fundamentals and applications.

In the present experiment, we have measured the emission spectra of forsterite single crystals under excitation with synchrotron radiation at low temperatures. In addition, excitation spectra were also measured for the observed emission peaks. The correction for the distribution of excitation light source was carried out for the excitation spectra observed.

Figures 1(a) and 1(b) show the emission spectra at 10K and 150K, respectively. In Fig.1(a), one can see the two emission peaks at around 2.60 eV and 2.82 eV. Since the 2.60 eV peak begins to quench thermally even at 10K, it cannot be found in Fig.1(b). The 2.82 eV peak is clearly observed at 300K. The other peaks below 2 eV may be connected to extrinsic origin, because their features vary for each sample. The excitation spectra for the 2.60 eV and 2.82 eV emission peaks are presented in Fig.2, together with the absorption tail spectrum. The threshold of excitation for the 2.60 eV peak is in good agreement with the fundamental absorption edge. This result indicates that the 2.60 eV peak is of an intrinsic of forsterite. The 2.82 eV peak is stimulated with ultraviolet photons below the fundamental absorption edge, and thus it originates in lattice imperfections. It is to be noted that both spectra resemble each other in the energy above 10 eV. This fact is explained as follows. The energetic *e-h* pairs produced by vacuum ultraviolet photons immediately relax into excitonic states. Excitons will migrate to be trapped at the sites of lattice imperfection. As a result, the 2.82 eV emission peak originates from the lattice imperfections excited. We thus suppose that the excitation of lattice imperfections by the inelastic scattering of hot photoelectrons is negligible in the energy region investigated here.

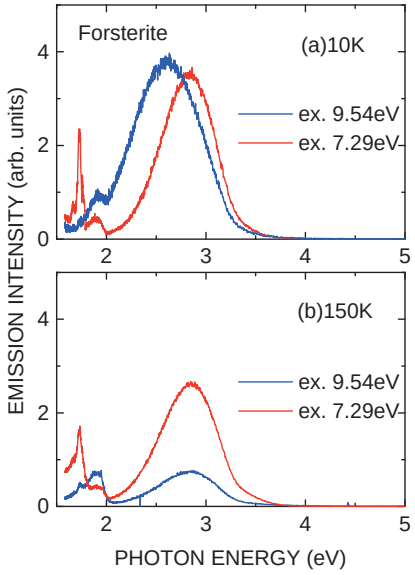

Fig.1: Emission spectra of forsterite at (a) 10K and (b) 150K. The red and blue lines correspond to the emission spectra measured under excitation below and above the fundamental absorption edge, respectively.

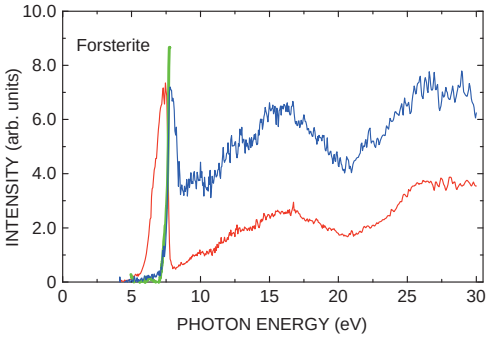

Fig.2: Excitation spectra for 2.60 eV emission peak at 10K (Blue line) and 2.82 eV one at 150 K (red line). The absorption tail spectrum at 10K is also presented by a green line for comparison.

[1] M. Kitaura *et al.*, J. Phys. Soc. Jpn. **71** (2002) 2736.